MEASUREMENT APPARATUS AND MODELLING OF LAMINAR BURNING SPEED AND MASS BURNING RATE OF SYNGAS AND ONSET OF AUTO-IGNITION OF N-HEPTANE AND GAS TO LIQUID FUEL

A Dissertation Presented

by

Mimmo Elia

to

The Department of Mechanical and Industrial Engineering

In partial fulfillment of the requirements
for the degree of

Doctor of Philosophy

in the field of

Mechanical Engineering

Northeastern University
Boston, Massachusetts

April, 2016

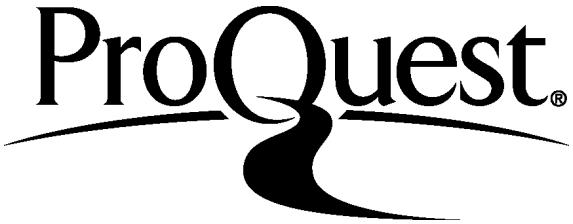

ABSTRACT

Research studies into understanding the fundamental thermodynamic properties of Syngas are extremely relevant in engineering combustion modelling for stationary turbine based power plants and for IC engines. The models rely heavily on accurate experimental results and of critical importance is the data for: chemical kinetic rates, mass burning rate and auto-ignition conditions. To produce some of this necessary data, an experimental facility capable of measuring the pressure rise from spherically expanding flames was developed. The first core component of the facility includes a spherical combustion vessel that enables the measurement of the pressure rise from a combustion process, at high initial temperature and pressure. The second core component of the facility, which includes a lower pressure cylindrical combustion vessel, with optically clear sides, enables the direct measurement of laminar flame speed as well as the visualization of expanding spherical flames for the study of flame structures. An improved model to complement the experimental measurements has been developed. Using the thermodynamic model, the mass burning rate and laminar burning speed can be calculated from the pressure data measured using one of the two constant volume combustion vessels. The model is used to calculate the mass fraction of the burned gas by simultaneously solving the conservation of mass and energy equations coupled with equilibrium concentrations calculation of the combustion products using STANJAN. For smooth non-cellular flames laminar burning speed can be also calculated. The facility and model have been used and improved by many of the researchers at Northeastern University with results published in a variety of technical journals, and thus expanding the measured range of laminar flame speed. This thesis will describe in detail the experimental apparatus and report the laminar burning speed and mass burning rate for Syngas-Air and Syngas-O_2-He at high temperature and pressure as well as auto-ignition characteristics of n-Heptane and GTL (S8), which is a synthetic surrogate for aviation fuel.

ACKNOWLEDGMENT

I would like to thank all whom have helped and supported me during the past several years. To my doctoral thesis committee members Prof. Behrooz Satvat, Prof. Reza Sheikhi and Prof. Mehdi Abedi it's been great to have had your encouragement these last few months, I really appreciate the time you have taken from your busy schedules. To my fellow researchers Omid Askari, Kevin Vien, Ziyu Wang thank you for all your help, sharing of ideas, information and patience, and a special thanks to Matt Ferrari for all the hard work, help and dedication on this research. To my fellow colleagues at Novatio, thank you for your understanding and extra effort. A special thanks to late Prof. James Keck for his lasting advice. Matthew Ulinski and Patrice Moore, thank you for all your help and early involvement in this project. Prof. Metghalchi, I would like to express a special thanks to you for all your good advice and motivation, not only during these last few years but throughout my academic studies at Northeastern University. You have been an excellent teacher and an even better advisor and friend; I have enjoyed working with you and I greatly appreciate all you have done for me. I feel honored to have worked with you and every one I previously mentioned. Finally, a very special thanks to my wife Erica, my kids Luca, Matteo and Liliana and the rest of my family for all their support, patience, encouragement and love throughout my life. I feel very lucky to have you by my side, encouraging and motivating me, I would like to dedicate this work to you.

TABLE OF FIGURES

1.0 INTRODUCTION

1.1 Introduction

The purpose of this research has been to design and develop an experimental facility capable of measuring the rate at which a mixture of fuel, oxidizer and diluent is consumed by a combustion process. To complement the experimental facility and utilize the pressure rise data produced during a combustion event, a thermodynamic model to calculate mass burning rate, has been developed. This model is an extension of the one which was developed by Metghalchi and Keck [1] [2] with the inclusion of burned gas temperature gradient from the compression of the combustion.

The experimental facility and combustion modelling described in this thesis has been widely used over the past years' researchers at Northeastern University and has produced an extensive amount of data that has helped expand the scientific knowledge of mass burning rate, laminar burning speed, flame stretch rates, auto-ignition characteristics for a wide variety of combustible mixtures. A list of the numerous publication is attached in Appendix 4.

The most recent set of experiments has focused on a set of new and interesting Synthetic Fuels and particularly on Syngas. A study to comprehensively measure and assess the mass burning rate (or mass burning speed) and onset of auto-ignition of Syngas (synthetic gas) is relevant and necessary to the scientific and engineering community [3] [4]. Syngas, a mixture of H_2 and CO, has gained importance as an alternative fuel for stationary gas turbines and internal combustion (IC) engines [5]. Power plants have been using Syngas for more than a decade, citing increased energy efficiencies and fewer emissions than traditional coal fired plants. Syngas is also increasingly being used in petroleum refineries to help produce cleaner transportation fuels and improve overall efficiency of the plant [6]. Syngas can be derived from the gasification of coal or biomass, including municipal waste, agricultural residue, and herbaceous energy crops therefore can help reduce greenhouse emissions.

Furthermore, utilizing a gas to liquid (GTL) process, refineries can convert their waste products into more versatile and useful liquid fuels [7]. GTL fuels are produced using the Fischer-Tropsch

synthesis method and can be synthesized into a variety of hydrocarbons chemicals. These GTL fuels can be surrogates for gasoline, diesel, and aviation fuels [8].

Research studies into understanding the fundamental thermodynamic properties of Syngas and GTL fuels are extremely relevant, particularly for use in engineering combustion modelling for stationary turbine based power plants and for IC engines in the transportation industry. The models rely heavily on accurate data which is usually gathered experimentally. Of critical importance to these models is the data for: chemical kinetic rates, mass burning speed and auto-ignition conditions [9].

Syngas mixtures have been well studied and researched at atmospheric and elevated conditions, however, measurements are missing at some relevant combinations of high temperatures and pressures (i.e Pressure >40atm, Temperature >750K) [10] [11] [12] [13]. Despite combustion engines being subjected to high pressures (>60 atm), few studies have been performed under comparable conditions. In a 2014 review of Syngas research, Lee concluded that new measurements on the burning speed and the auto-ignition were needed at elevated pressures [14]. Both mass burning rate and the auto-ignition point are fundamental parameters used in the modeling of combustion systems.

A comprehensive literature search of burning speed measurement of all Syngas compositions exposed various gaps in the experimental data especially at elevated temperature and pressure conditions [14]. Some data exist but doesn't comprehensively capture the whole range of conditions between 1-80 atm and 300 -~750K, with varying degree of stoichiometry and gas mixture compositions. Similarly, data for the on-set of auto-ignition for Syngas mixture has not comprehensively been measured [15].

1.2 Measurement techniques for mass burning rate and auto-ignition

Mass burning rate and auto-ignition are important thermo-physical property of every combustible mixture [16]. Mass burning rate is the rate at which a combustible mixture is consumed by a flame front. When the flame front is laminar and its area is known a more commonly used term to describe this property is laminar burning speed [17]. Mass Burning Rate (MBR) is a measure of the energy release during a combustion process and is often used to validate chemical kinetics models [18]. A variety of measurement techniques for MBR exist and can be generally classified into two categories: stationery or propagating flame. Detailed reviews of the different techniques can be found in the literature such as Andrews and Bradley [19] and Rallis and Garforth [20]. "Propagation of spherically expanding flames in closed vessels has been subject of many theoretical and experimental studies in the past few years. Investigation of spherical flame propagation either in constant pressure or rising pressure regimes is recognized to be one of the most accurate approaches for laminar burning speed measurement and flame structure study. [21]

The auto-ignition point of mixture or the on-set of auto-ignition is the set of thermodynamic conditions of at which the combustion process spontaneously and simultaneously occurs throughout the combustible mixture [22]. For any particular mixture of fuel, oxidizer and diluent, the temperature and the pressure are the key parameters to consider as the drivers to auto-ignition [23]. Time is also a factor in driving auto-ignition, and typically a parameter called ignition delay can be experimentally determined as the time a mixture may remain at a temperature and pressure before auto-ignition occurs [24]. Typically, rapid compression machines or shock tubes are used in determining the auto-ignition characteristics of a mixture. These techniques both rapidly increase the pressure of a mixture to a specified value then the eventual pressure spike from an auto-ignition event is detected by a pressure transducer, any lag between the induced pressure of the experimental apparatus and the auto-ignition pressure spikes is characterized as ignition delay [4]. The results from such experiments even though widely accepted do not represent the conditions typically found in practical applications of combustion system where the pressure and temperature of a mixture are constantly changing. Using the experimental facility described in this thesis a controlled combustion event in one of the constant volume combustion vessels produces an increase in the pressure and temperature of the unburned mixture [25]. When auto-ignition conditions are reached

in the unburned gases the whole mixture instantly and simultaneously ignites to produce a series of pressure waves that can be detected by the pressure transducer. The conditions of the unburned gases that initiate the pressure waves are the conditions at which auto-ignition occurs, and are more representative of the varying conditions typically found in a practical combustion system such as an internal combustion engine.

2.0 EXPERIMENTAL FACILITY

2.1 Experimental Facility Overview shown below on Figure 1

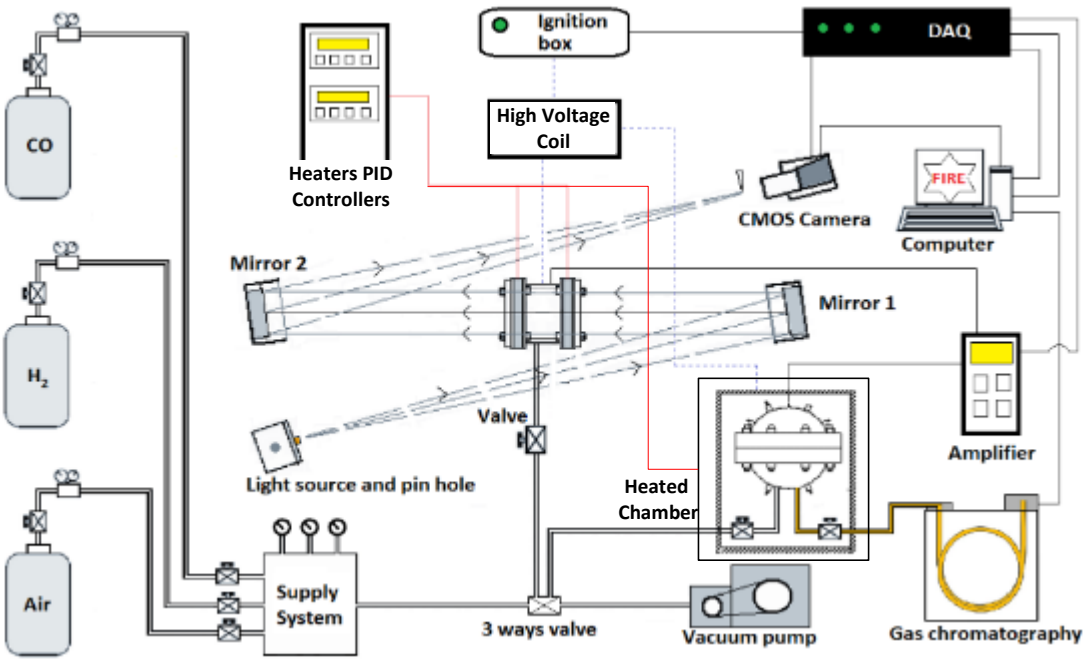

Figure 1: Overview of experimental facility

The experimental facility has been optimized for efficiency, versatility, safety and ease of use, as to make the transition to future researches as seamless as possible. Over the many years of running experiments and tweaking the systems and processes, the current laboratory facility is considered state of the art. All the data acquisition and analysis can be done on-site by several dedicated PCs using a high speed LabVIEW DAQ card and isolated input and output modules for temperature, voltages and pressure measurements as well as automatic delayed firing via control of the high voltage coil driving the spark plugs. The filling manifold mainly constructed of 304 and 316 Stainless steel Swagelok componentry and tubing is predisposed to accommodate inputs from 5 simultaneous gas cylinders, thus allowing for an inventory of gas mixtures to be always readily available for immediate use. Two vacuum pumps help evacuate the system faster and allow for

independent testing of the two vessels. The heater controllers are proportionally programmable with redundant safety features for over temperature protection and electric shock. The cylindrical vessel with optical side ports and all its supporting system are rigidly mounted to a heavy optical bench. Using a focused light source and a series of mirrors, the light is guided through the optically clear Quartz sides and reflected to a high speed CMOS camera capable of capturing images at 40,000 frame per second. This shadowgraph effect is useful in visualizing the flame propagation, as well as investigating the shape of the flame front. Another key element of the apparatus is the liquid filling system where a slug of liquid fuel is allowed to enter and evaporate in a temperature controlled portion of the manifold. A higher temperature pressure transducer closely coupled to this section of the manifold is used to monitor the partial pressure of the vaporized fuel and hence control the amount of fuel that will be used in the experiment.

2.2 Combustion Vessel

The combustion vessel, shown in Figure 2, is constructed from two hemispheres 1 inch thick that are bolted together at their flanges with six bolts of 0.75 inch diameter to give a 6 inch spherical vessel that can withstand 425 atm of pressure. The size of the vessel was optimized by Metghalchi [1] to satisfy the following requirements. “It is of course also desirable to keep the size of the combustion bomb small for convenience in machining and operating the apparatus” Metghalchi [1]. The vessel is fitted with two ports for the sparkplug electrodes, one for the piezoelectric pressure transducer (Kistler model 601B), one for filling and three additional ports that can be used either for ionization probes or thermocouples. In the current set up three ports are used with ionization probes, two mounted equidistant from the top of the vessel and one diametrically opposed to one of the top probes. The location of the ports was strategically chosen to allow the measurement of buoyancy and ignition misalignment. The cylindrical vessel, shown in Figure 3, was designed with the same features as the previously described spherical vessel, however, for ease of construction and to maintain high pressure rating (50 atm) the diameter was reduced to 5.3 inch (13.5 cm). The ends of this vessel are 1.5 inch thick, 6.5 inch diameter discs made from fused silica, chose for their extremely high optical clarity and shock strength.

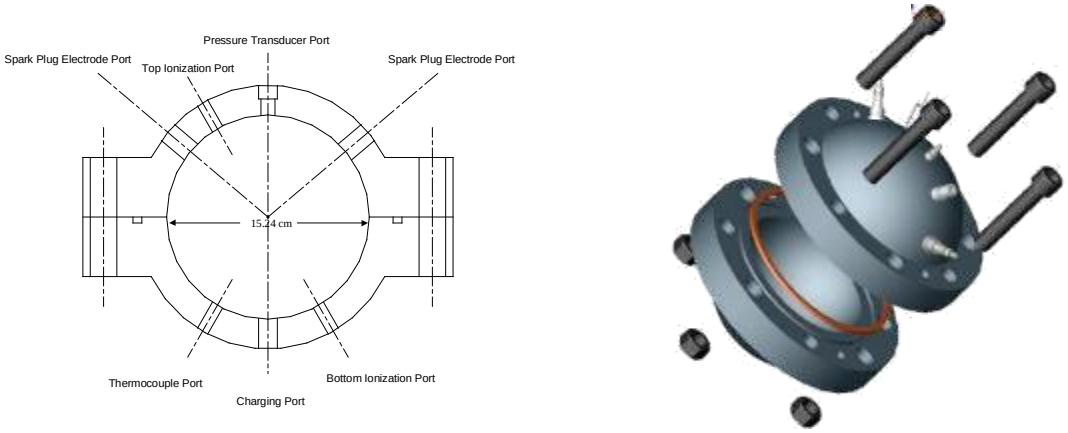

Figure 2: Diagram of Spherical Vessel and the placement of the ports.

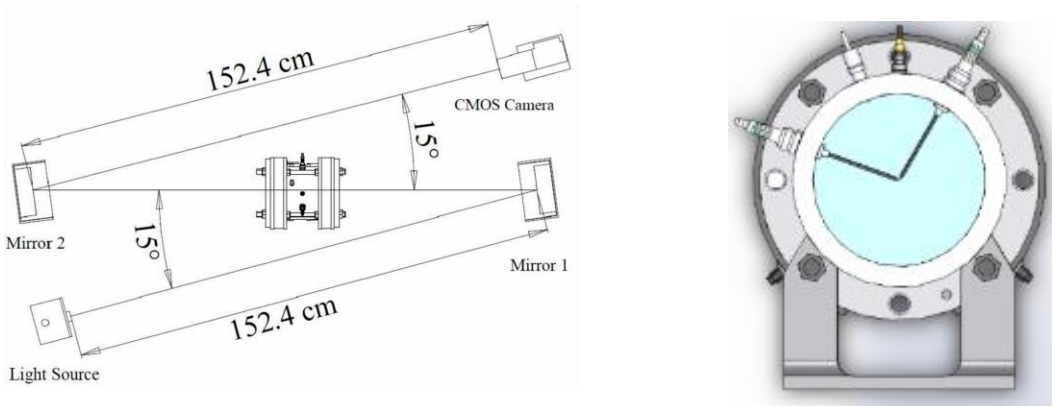

Figure 3: Diagram of Cylindrical Vessel

2.3 Partial Pressure filling system and Gas Chromatograph

The partial pressure filling method is used to quantify the amount of the desired gas constituents in any given experiment. The method is based on the ideal gas law where the partial pressure of a gas represents the molar fraction of the same gas in a mixture. Special care has to be taken in the sequence of the filling process by filling the gases in order lowest to highest partial pressure. A typical process starts by vacuuming down the vessel and all the filling manifold to a pressure less than 200 mTorr to ensure no residual gases remain in the system and potentially influence the measurements (500 mTorr was determined not to influence the results of the

experiments). A spreadsheet model to calculate the desired amount of fuel, oxidizers and diluent as a function of the desired Stoichiometry and initial Pressure was created (Figure 4). Any offset of the pressure transducers at <0 atm is also accounted for in the calculation and the partial pressure of the gases is determined as well as model of pressure transducer to use.

Figure 4: Partial pressure calculator spreadsheet

A wide range of initial pressures are usually required for a comprehensive parametric study, therefore, five pressure transducers of varying ranges (0-5, 0-15, 0-30, 0-150,0-250 psia) are used in the filling manifold to optimize the accuracy of the measurements. The filling mixture is spot checked with a gas chromatograph (Figure 5) for any potential inconsistency and to confirm operation of the pressure transducers. In order to ensure proper initial mixture, the same experiment is repeated at least twice, and only if the resulting combustion pressure curves are an exact match is the data considered. Aside from human error or malfunctioning equipment this process is very repeatable.

Figure 5: Image of partial pressure filling system and Gas Chromatograph

2.4 Extended spark plug electrodes

Two standard 14-mm spark plugs have been modified to ignite the mixture in the vessels. The electrodes of these spark plugs have been center drilled to accept approximately 0.020inch of a long stainless steel rod (0.020-0.06-inch diameter). The rod perfectly aligned with the spark plugs via the centered drilled hole is then welded to the sparkplug electrode via laser welding creating an extended electrode spark plug. The end of the steel rod has been sharpened to a point and used to form the spark plug gap at the center of the vessel with a gap of approximately 2 mm. The figures below (Figure 6 and Figure 7) show how the two extended spark plug electrodes are used in the vessels.

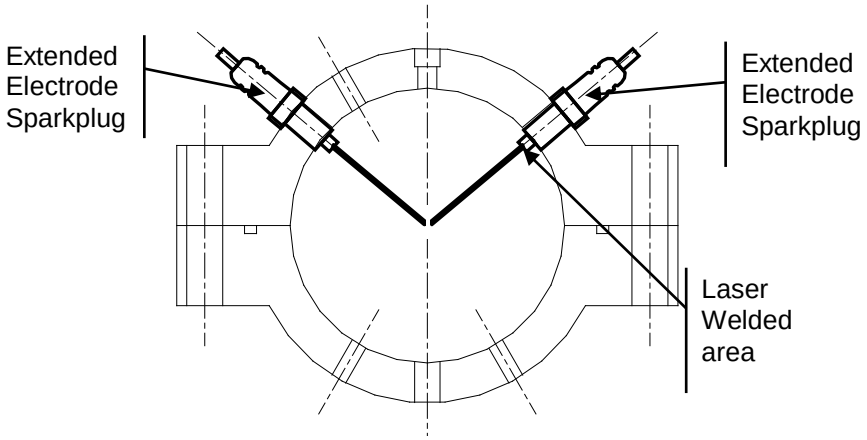

Figure 6: Schematic of the extended electrode spark plugs installed in the spherical vessel

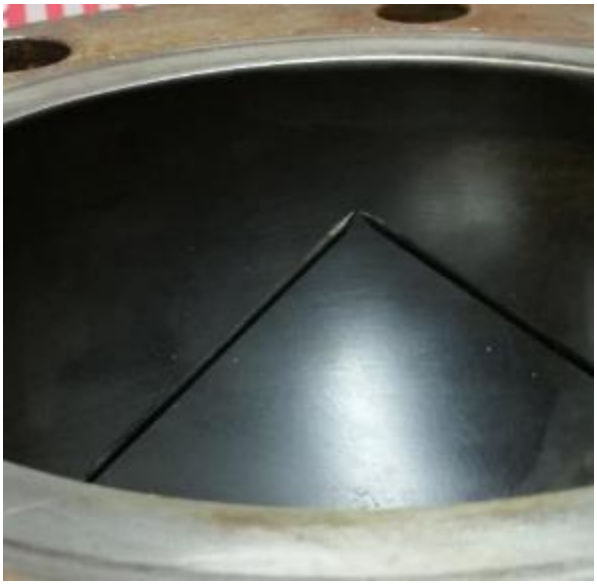

Figure 7: Picture of the extended electrode spark plugs installed in the spherical vessel

2.5 Ionization probes

The purpose of an ionization probe is to signal the arrival time of the flame front by measuring the current flow through the ions present in the flame and not in the unburned gases. By mounting the ionization probes flush with the inner surface of the combustion vessel, they will indicate the flame arrival time at the wall of the vessel. This information helps determine if

the mixture was ignited at the center of the vessel by the extended spark plug electrodes and the effect of buoyancy.

The Ionization Probes are constructed using a 1/8 inch diameter Swagelok tube to NPT adapter fitting. These were drilled through to accommodate a 1/8 inch Teflon insulating tube with a 1/16-inch stainless steel rod through it. The rod and Teflon insulation were swaged to the fitting creating essentially an airtight electrically isolated feed-through. The assembled Ionization probe is machined to size as to protrude ~ .020 inch beyond the inner surface of the vessel once installed. The final product shown in Figure 8 provides approximately a 0.03 inch gap between the rod and ground (the fitting and vessel are electrically grounded).

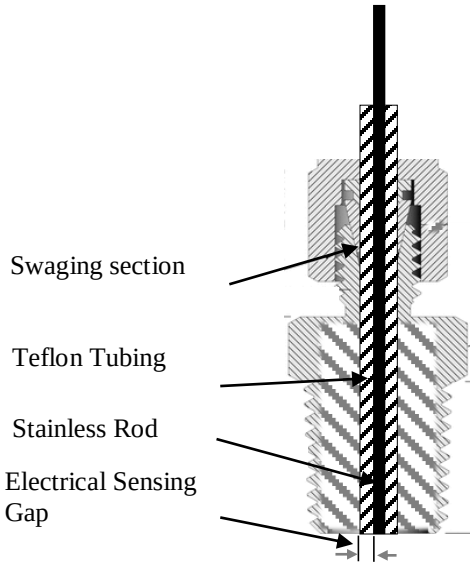

Figure 8: Ionization Probe Construction

Complementary to the mechanical development of the Ionization Probe is the electronic circuitry to process the signal. The ionization probe is designed and positioned to detect the eventual flow of current across its gap. A voltage potential is present across the gap and drives a current flow when ions are present in the vicinity. Since the flame front has a high concentration

of ions, a detectable current starts to flow when the flame arrives at the probes gap. The circuit shown below (Figure 9) detects a current flow and outputs a sharp voltage transient.

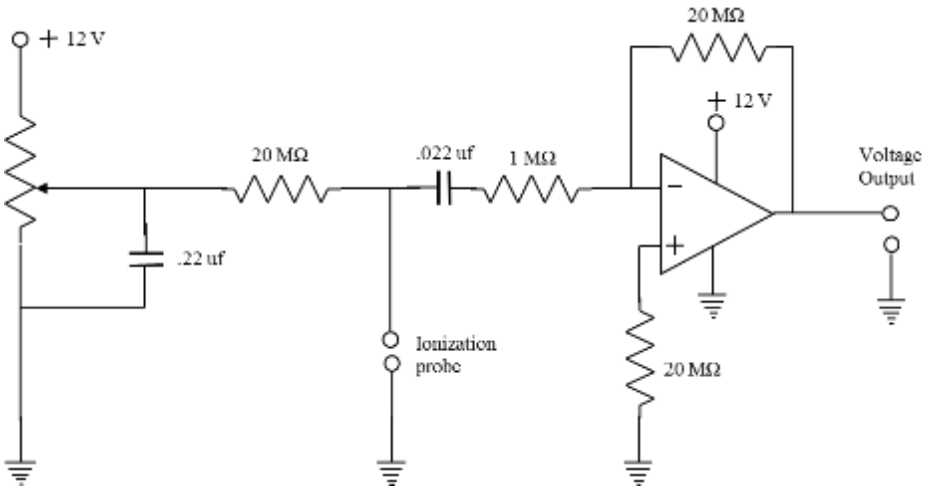

Figure 9: Ionization probe circuit schematic

2.6 Ignition system

A capacitor discharge ignition system was developed to produce a high voltage signal with a selectable amount of charge, that will arc across the extended spark plug electrode to ignite the mixture inside the vessel. The capacitor discharge is timed and controlled by the LabView data acquisition system via an isolated SCC-DO01 module to prevent damage from eventual high voltage spikes. With enough resolution on the chosen set of capacitors this system can be used to determine the minimum ignition energy of a mixture. An electrical schematic of the ignition system is shown in Figure 10.

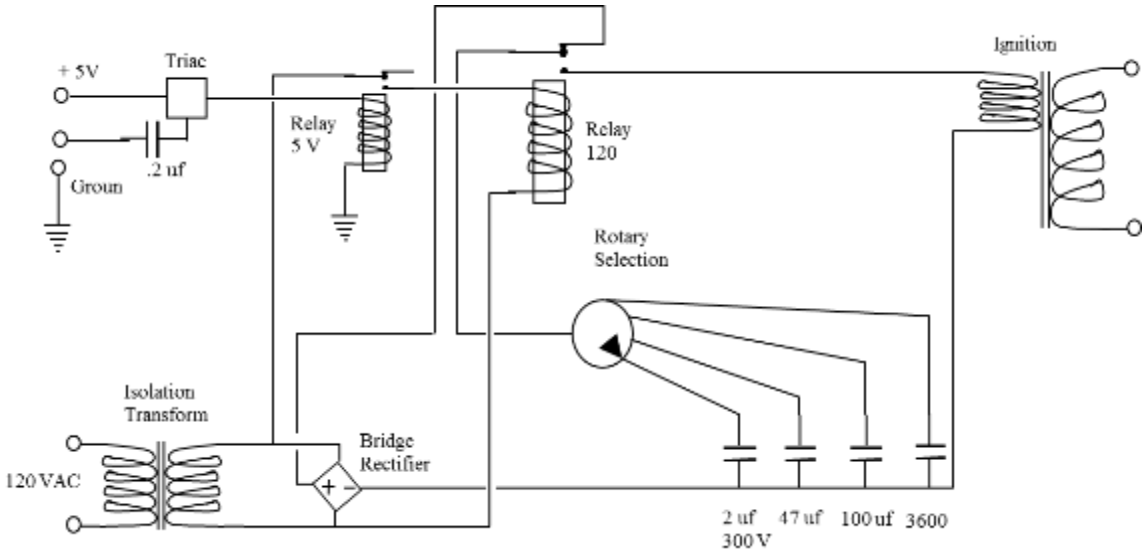

Figure 10: electrical Schematic for Capacitor discharge ignition system

2.7 Data acquisition and other supporting electrical systems

The data acquisition system consists of a lab PC with LabVIEW PCI DAQ card , a SC2345 (signal conditioning enclosure) and a series of signal conditioning modules. The input voltage modules (mod SCC-FV01) used for the pressure and ionization probe signals are capable of measuring up to 10V and provide voltage isolation. The output modules (model SCC-DO01) are used to trigger the Ignition system and the CMOS camera. The 16Bit PCI data acquisition records the pressure change of the combustion event at a rate of 10kHz as well as the two ionization probes mounted diametrically opposed to each other. All signals are processed by the lab PC and output data file is automatically generated. Figure 11 shows the graphical user interface and Figure 12 the recorded data from two consecutive experimental runs.

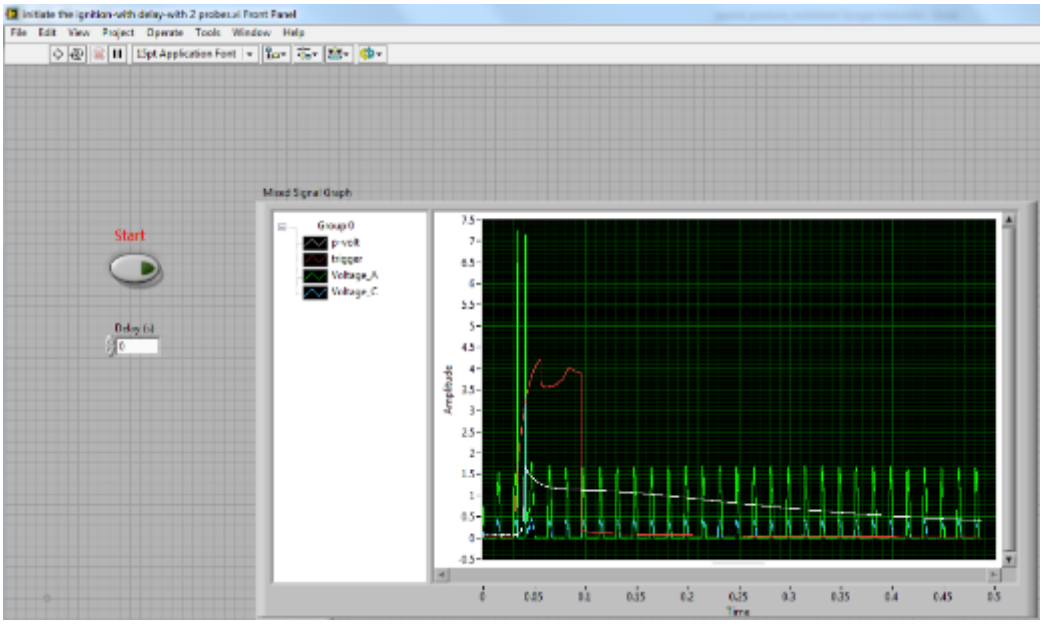

Figure 11: LabView data-acquisition graphical user interface

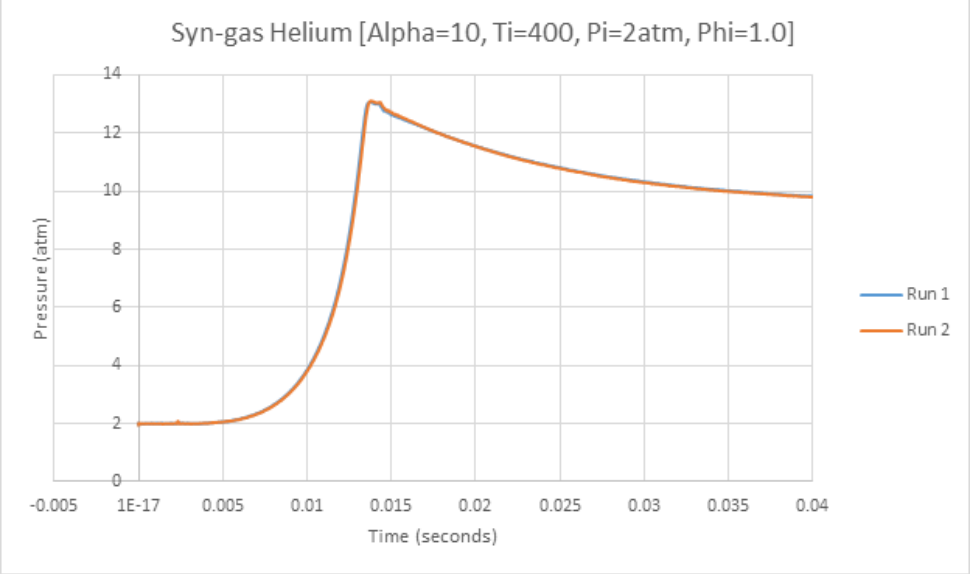

Figure 12: Typical output data from two experimental runs

2.8 CMOS high speed camera

The camera in use, shown in Figure 13, is the MotionXtra HG-LE by RedLake. The camera is capable of taking up to 100,000 frames per second. The camera is mounted to a slide table, which allows for fine adjustments by micrometers heads. The slide table is a purchased part, series 4412, made by Parker.

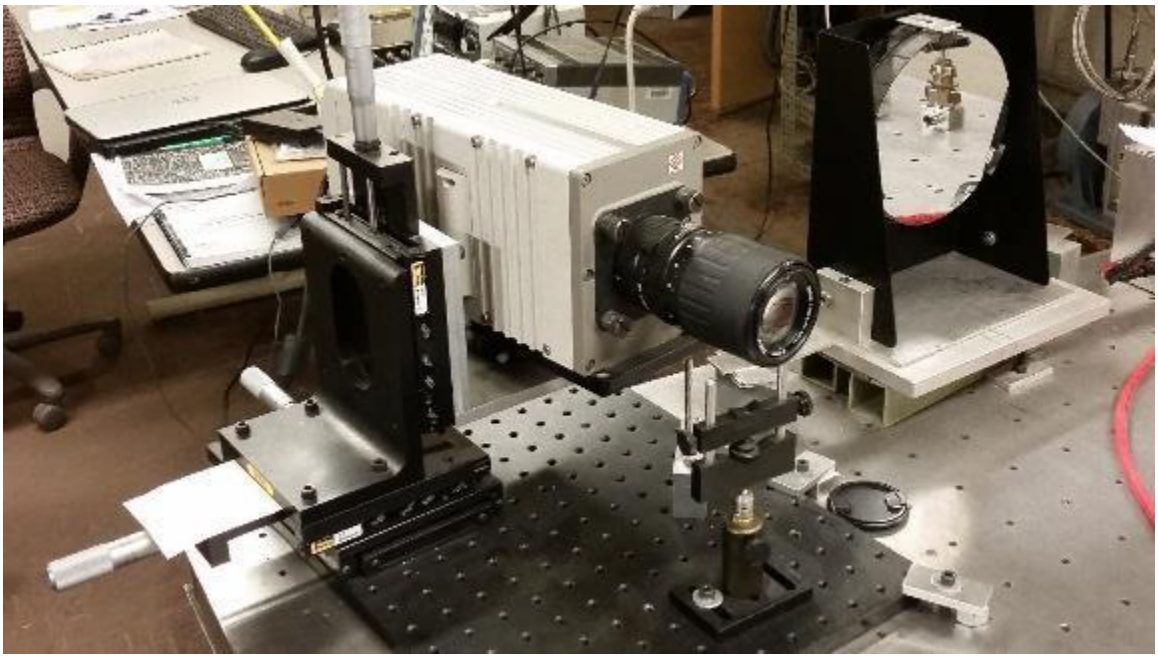

Figure 13: High Speed Camera

2.9 Oven and heaters

Several key experimental components are required to operate at high temperature when high initial temperature experiments are desired. The combustion vessels and portions of the manifold feeding it are required to be heated.

The cylindrical vessel is heated using two band heaters around the outer most cylindrical portion and insulating the remaining cylindrical body with ceramic fiber insulation, thus leaving the two end with the clear glass sides exposed. The band heaters, made by TempCo, are 120V and 1500 Watt heaters. Since the glass is a good thermal insulator, this approach works very well and the vessel can be effectively and efficiently heated. A picture of the cylindrical vessel and band heaters is shown in Figure 14.

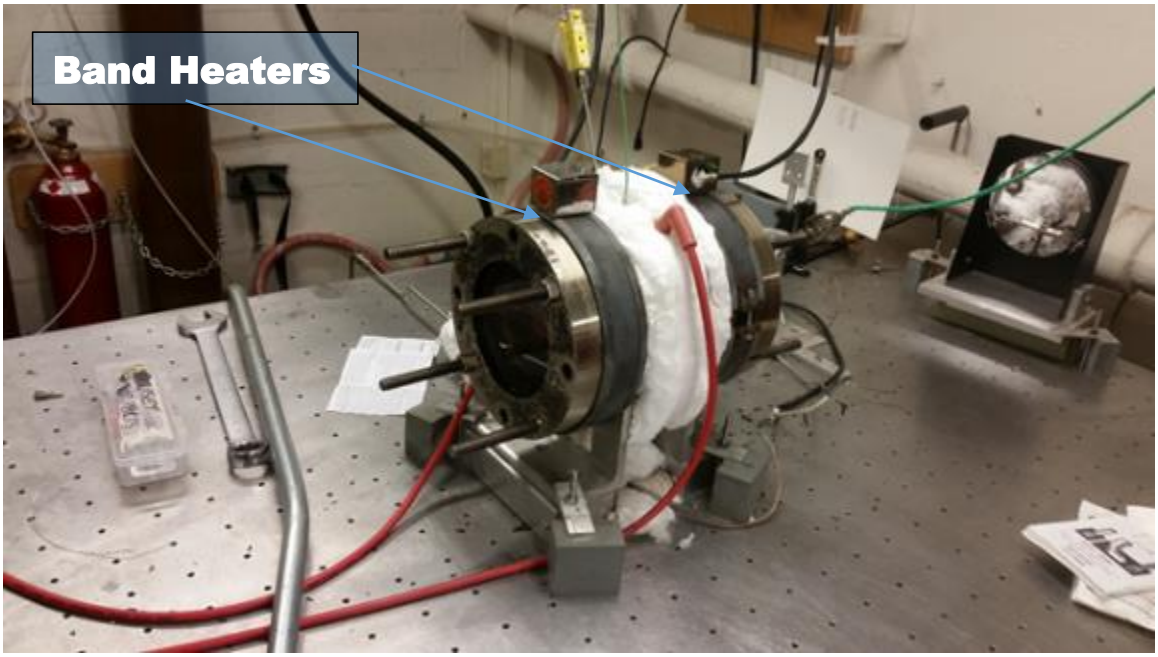

Figure 14: Picture of cylindrical vessel with band heaters

The spherical vessel does not lend itself to be heated by band or strip heaters, therefore, an oven chamber was designed and developed for the purpose of housing and heating the entire vessel. The oven is constructed of two hollow cylindrical half chambers with high power heating elements embedded in its ceramic liner, shown schematically in Figure 15 and photographed in Figure 16. The two half chambers are hinged along one side to swing close and create a hollow cylindrical cavity that houses the combustion vessel and all its peripheral components. Two thermocouple extend form the oven walls into the cavity, one is used for temperature control the second as a high limit safety.

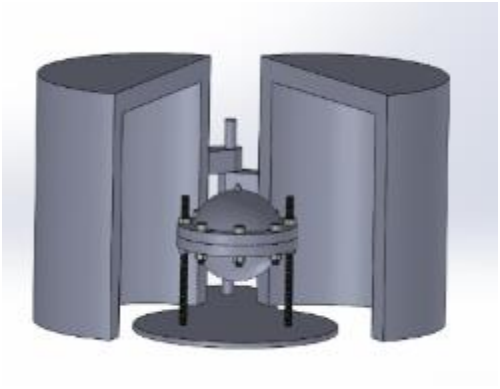

Figure 15: Schematic and picture of the custom oven used in heating the spherical vessel.

Figure 16: Closed Custom Oven

The heated manifolds for vaporizing liquid fuels were developed using cartridge heaters embedded in thick walled aluminum channels machined in the appropriate shape as to house the manifold, several valves, a pressure transducer and safety relief valve. A thermocouple is mounted to the portion of the filling lines that contain the fuel to be vaporized in conjunction with a proportional temperature controller the desired temperature is maintained in the filling lines feeding the hot vessels. A picture of the liquid filling lines is shown below on Figure 17.

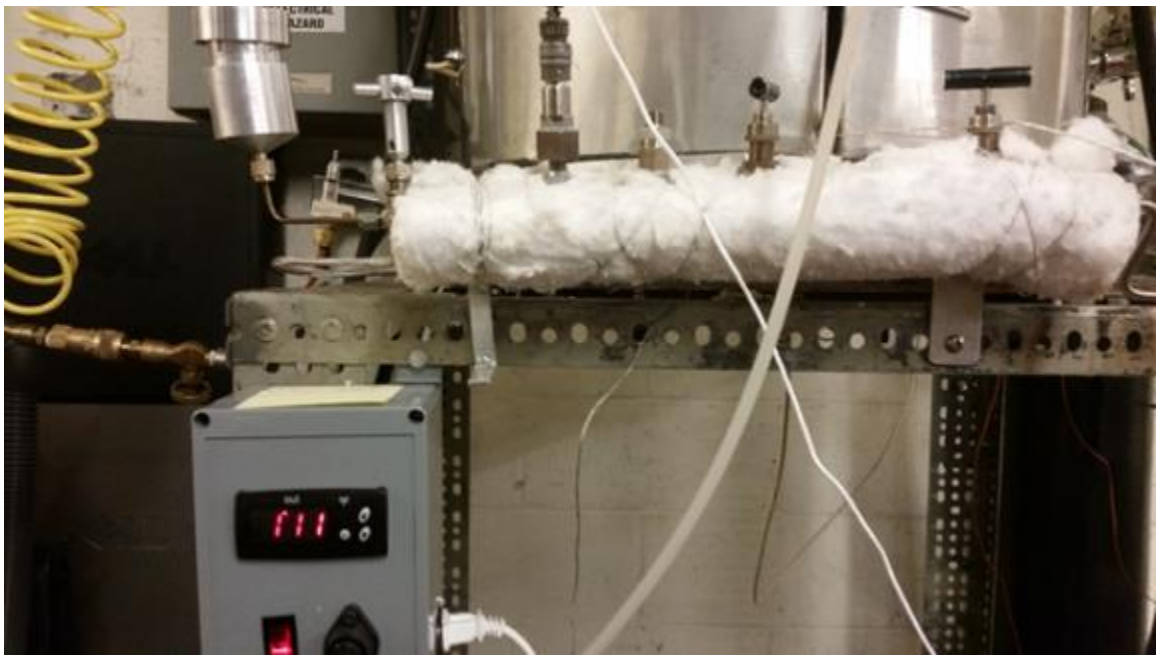

Figure 17: Heated liquid filling lines and controller

The band heaters, cartridge heaters, and oven are all controlled using proportional temperature controllers. K-type thermocouples are used for the temperature readings and high power solid state relays are used for high current switching.

3.0 MODEL

The thermodynamic model first developed by Metghalchi and Keck [1] with some improvements is used here for the determination of mass burning rate. The original model considers the gas in the vessel as composed of two main parts, one part burned gas, at the core of the vessel and one part unburned gas surrounding the core. The burned gas expands into the unburned gas and consumes it. The proposed improvements to this model account for thermal gradients in the burned gas. Evaluation of the burned gas properties is executed using the well accepted third party chemical equilibrium code (STANJAN). Evaluation of the unburned gas properties is executed using the JANAF (NASA) tables. A schematic of the model is shown in Figure 18.

Figure 18: Schematic of thermodynamic model

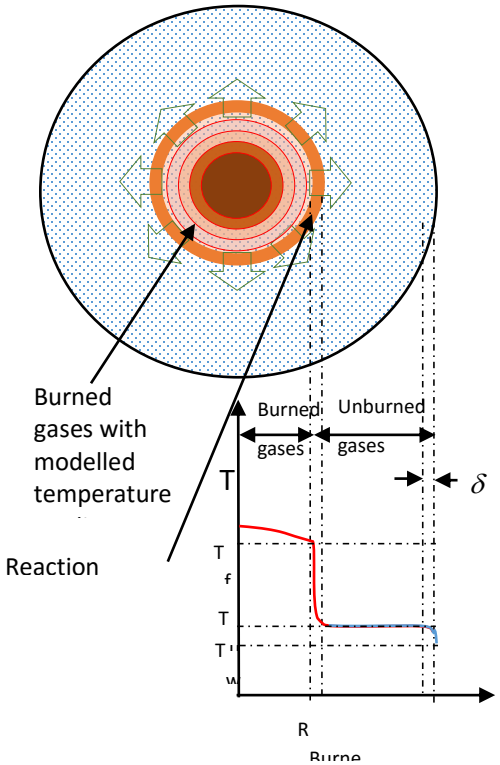

In this model, two non-linear conservation equations, the conservation of mass and the conservation of energy equation, are solved simultaneously for the unknowns: mass fraction of the

burned gas and temperature of the burned gas. In addition, a numerical derivative of the pressure time data can be calculated and used to correlate the onset of auto-ignition.

The effect of flame stretch rate has been shown to be small (Appendix 2)) and it has been neglected. In this model, two non-linear conservation equations, the conservation of mass and the conservation of energy equation need to be solved to yield the mass fraction of the burned gas.

$$\frac{V}{m} + \frac{A\delta}{m} = \int_0^x v_b dx' + \int_x^1 v_u dx' \qquad (1)$$

$$\frac{E}{m} - \frac{Q}{m} = \int_0^x e_b dx' + \int_x^1 e_u dx' \qquad (2)$$

Where:

A = combustion vessel wall area

e = specific internal energy

E = total initial energy of gas in the vessel

m = mass of gas in the vessel

Q = total energy transfer from the boundary layer displacement thickness to the vessel wall

x = mass fraction burned

x' = integration variable

v = specific volume

V = combustion vessel volume

δ = boundary layer displacement thickness

and the subscripts *b* and *u* refer the to burned and unburned gas respectively. The boundary layer displacement thickness is defined as:

$$\delta = (1/\rho_\infty)\int_0^\infty (\rho - \rho_\infty)dr \qquad (3)$$

Where:

ρ = density of unburned gas within the boundary layer displacement thickness

ρ_∞ = density of that portion of unburned gas that compresses isentropically

Metghalchi and Keck [11] calculated the boundary layer displacement thickness using the pressure signal:

$$\delta(t) = \left(\frac{\mu_0}{\pi\rho_0}\right)^{\frac{1}{2}}\left(\frac{\rho_0}{\rho}\right)^{\frac{1}{\gamma_u}}\int_0^t\left[\left(\left(\frac{p'}{p_0}\right)-\left(\frac{p'}{p_0}\right)^{\frac{1}{\gamma_u}}\right)\left(\int_{t'}^t \frac{p''}{p_0}dt''\right)^{-\frac{1}{2}}\right]dt' \qquad (4)$$

where:

ρ_0 = the intial denisty of the gas mixture

μ_0 = the viscosity of the unburned gas at the intial temperature and pressure

γ_u = the specific heat ratio of the unburned gas

p_0 = the intial pressure of the gas mixture

p', p'' = instaneous pressure

t = time

t', t'' = integration variables

Energy transfer at the boundary to the vessel wall causes the displacement thickness temperature to be lower than the rest of the unburned gas. Therefore, the displacement thickness gas density is higher. Assuming this displacement thickness has the same properties as the core gas, the volume of the vessel must be increased by $A\delta/m$ to account for this density difference. Total energy transfer to the bomb wall is then calculated as Metghalchi and Keck [1].

$$Q = A\int_0^{\delta} p d\delta' \tag{5}$$

Where,

δ' = integration variable.

The two conservation equations (1,2) can be solved numerically for the mass fraction burned. Once the mass fraction burned (x) is known as a function of time it can be differentiated numerically to obtain $\dot{x}$ and hence Mass Burning Rate (MRB) by multiplying by the total mass in the system (MBR= $m\dot{x}$).

When the flame is smooth, un-stretched and non-cellular then the Laminar Burning speed can also be calculated, however, in the experimental runs of interest in this study only some of the low initial pressure test runs fall into this category [26]. The following equations are used to calculate Laminar Burning Speed:

$$S_u = mv_u \dot{x} / A_f \tag{6}$$

Where:

$\dot{x}$ = rate of mass fraction burned

A_f = the area of the flame = $4\pi R_f^2$ (7)

and, R_f, is the radius of the flame front:

$$R_f = \left(3V_b / 4\pi\right)^{1/3} \tag{8}$$

This is calculated from the volume of the burned gas:

$$V_b = xv_b m \tag{9}$$

4.0 ANALYSIS OF PRESSURE-TIME DATA

4.1 Processing of pressure signal data

The raw pressure signal produced by the high speed pressure transducer contains digitization noise resulting from data acquisition system process of converting a voltage signal to a digital value. The digitization noise is approximately 0.25 psi /bit which is certainly negligible for the range of pressure measurements of interest (<<1%) however, to avoid convergence errors in the computational model the pressure data is processed using a five point moving average, the resulting "smooth" pressure is shown below in Figure 19:

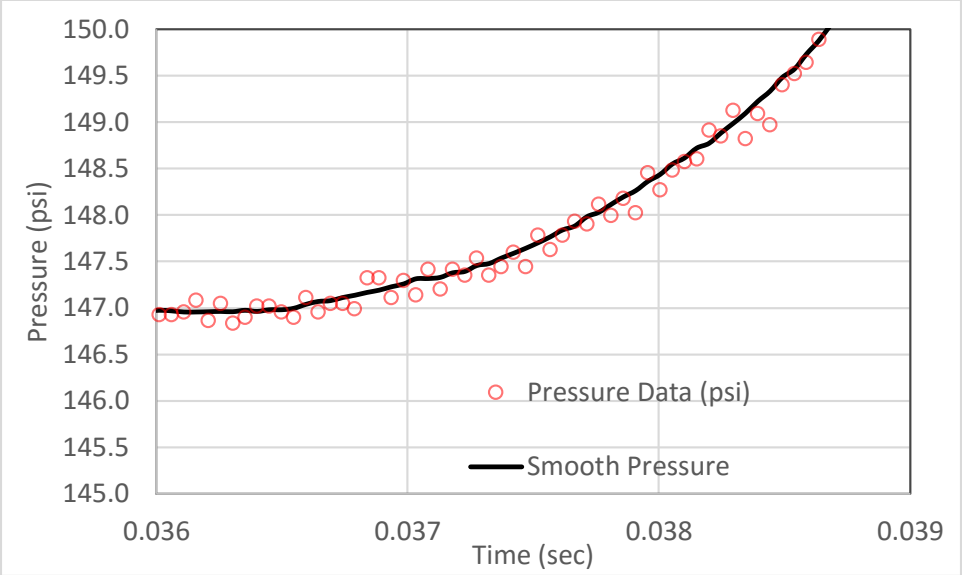

Figure 19: Raw and smoothed pressure signal

To minimize other experimental or human errors, a data selection criteria was developed. For any set of data to be deemed acceptable two consecutive experimental runs have to yield the "exact" pressure curve (within a small tolerance). The data from two or more runs is analyzed using a customized spreadsheet template thus allowing the operator to quickly determine if the data meets the acceptance criteria. The excel spread sheet first aligns the starting points of the runs based on the measured spark signal, which is the initiation of the combustion event. Then the time of the

top ionization probes signals for the respective runs is used as the end point of the data. The ionization probe signals indicate the moment the flame front reach the vessel's wall, since at this point the modelling assumptions are no longer valid, the data beyond this point is cropped. Finally, two or more resultant pressure curves are plotted together and visually inspected. Typically, the curves that pass visual inspection are within 1% of the average values of the runs (the data closest to the average is used). The results of the start-aligned data using the custom spreadsheet is shown on Figure 21 and the cropped data on Figure 22.

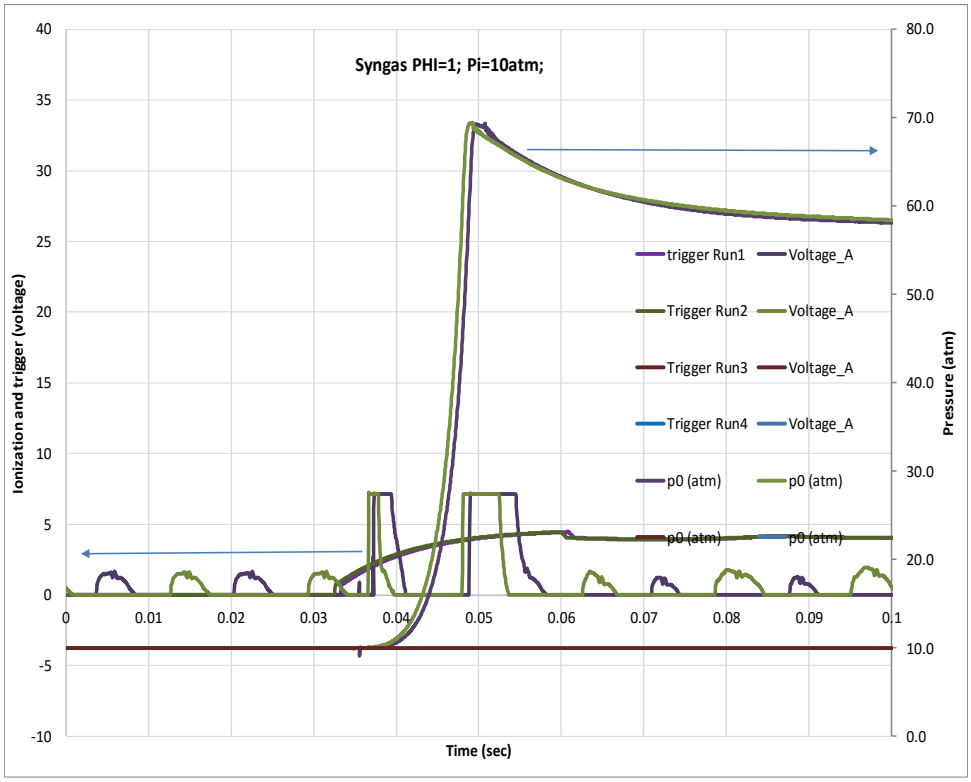

Figure 20: Pressure, trigger and Ionization signal data

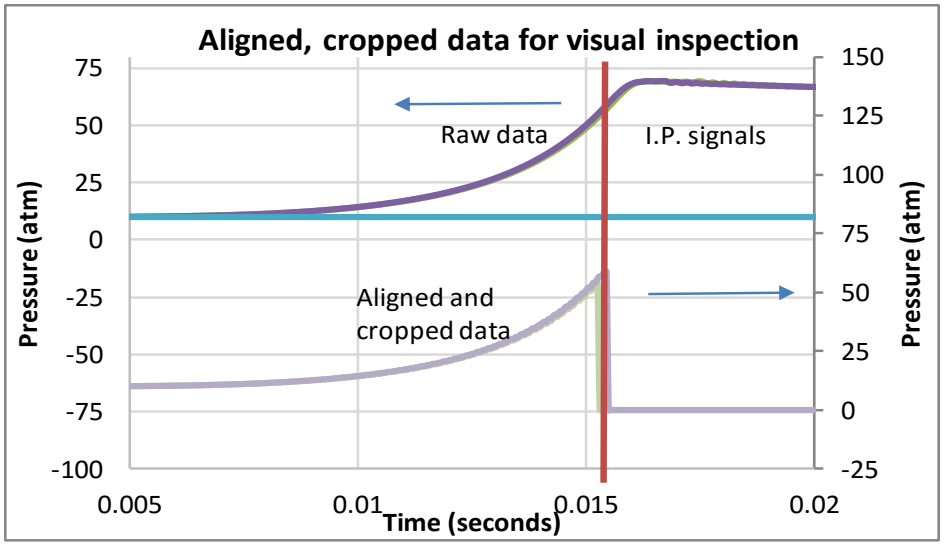

Figure 21: Aligned and cropped data for visual inspection

The importance of cropping the data using the Ionization probe signals or using the inflection point of the pressure data is demonstrated in Figure 21. Once the flame makes contact with the wall of the vessel, the rate of pressure rise decreases, this is the effect of energy losses to the vessel's wall from the hotter burned gases. Figure 22 demonstrates that the effects of the energy loss to the walls are more significant in the cylindrical vs spherical vessel due to the larger surface to volume ratio of the cylindrical shape.

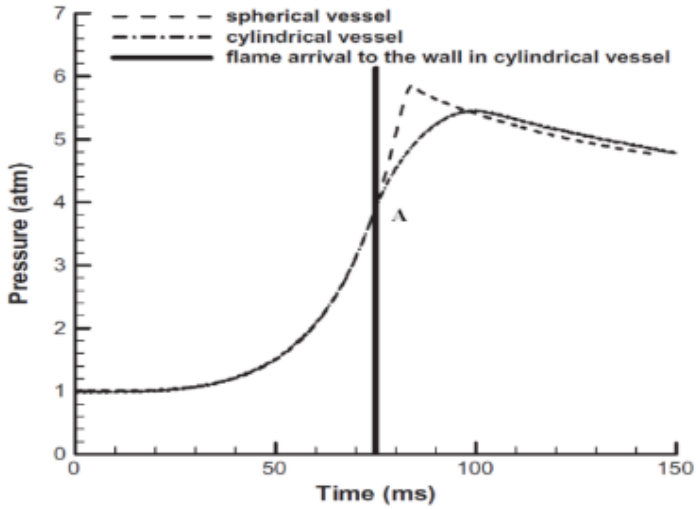

Figure 22: Comparison of flame arrival time in cylindrical vs. spherical vessel [21].

4.2 Analysis of pressure-time data

The pressure-time data is end goal of the all the intricate experimental set-up and careful testing. To an experienced researcher in this field of combustion the shape of the pressure-time curve can give instant insight to the characteristics of the event. A sharp fast rising curve is an indication of a rapid burning flame front, whereas a slow curve with a large portion of data post inflection indicates a slow burning flame with buoyancy driving the flame to quench on the top wall of the vessel, a sharp oscillating curve indicates auto-ignition.

Using the isentropic compression assumption, the unburned gas temperature can be calculated just from the pressure data and knowledge of the initial conditions. Having calculated the unburned gas temperature as a function of pressure and hence time, all the other thermodynamic properties of the unburned gas can be calculated using equation 10 with exact specific heats given by JANAF tables and equation 11.

$$\int_{T_1}^{T_2} C_p dT = \int_{P_1}^{P_2} R \frac{dP}{P} \tag{10}$$

$$C_p = R\left(c_0 + c_1 T + c_2 T^2 + c_3 T^3 + c_4 T^4\right) \tag{11}$$

The other unburned gas properties, specific internal energy and specific volume are calculated using the unburned gas temperature by the following equations.

$$e_u = \left(c_0 + c_1 \frac{T}{2} + c_2 \frac{T^2}{3} + c_3 \frac{T^3}{4} + c_4 \frac{T^4}{5} + \frac{c_5}{T} \right) RT - RT \tag{12}$$

$$v_u = \frac{RT}{P} \tag{13}$$

Equations 11 and 12 are valid for each particular species in the unburned gas mixture given the corresponding coefficients (c_0-c_5). A molar average specific heat and specific internal energy are then computed and are used in unburned gas calculations (details of molar averaging are found in (Appendix 3).

An accurate analysis of the experimental results also requires that the heat transfer from the unburned gas to the wall of the vessel is evaluated. Equations 4 and 5 are numerically integrated, and therefore the displacement thickness and energy transfer are calculated as a function of pressure (and hence also time) in each experimental run.

The boundary layer displacement thickness and the total heat transfer to the wall have been calculated using equations 4 and 5. Figure 23 and Figure 24 indicate the variation of displacement thickness and heat transfer vs. the normalized flame radius for stoichiometric Methane experimental run at initial pressure of 1atm and initial temperature 298 K. As Figure 23 and Figure 24 indicate, both the correction for the volume equation by the displacement thickness and to the energy equation by the heat transfer are extremely minor < .5%.

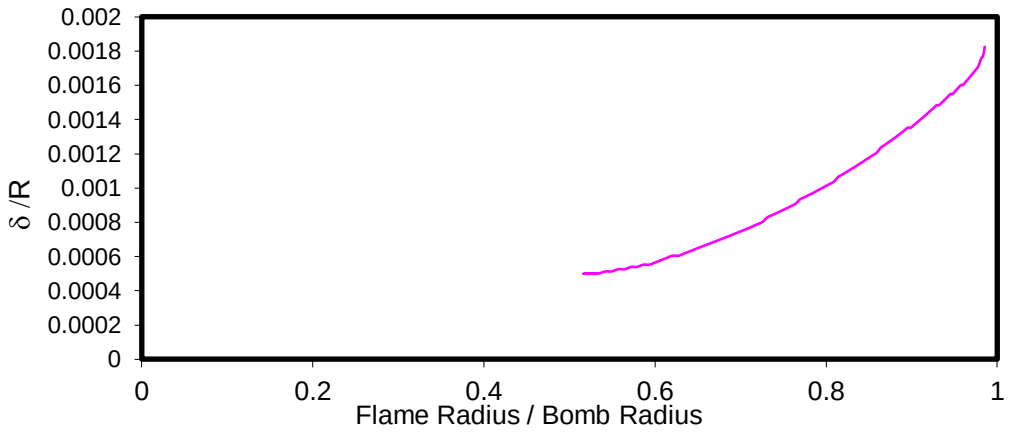

Figure 23: Normalized Displacement Thickness vs. Normalized Flame Radius

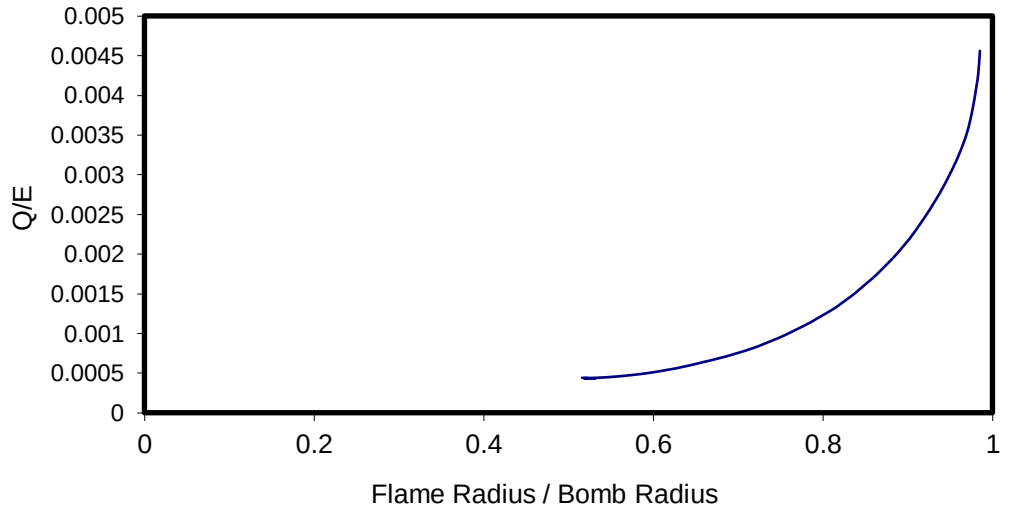

Figure 24: Normalized heat transfer vs. normalized flame radius

Evaluation of the unburned gas properties, energy transfer and displacement thickness leave the burned gas properties as the unknowns of the two conservation equations (equations 1 and 2). The total properties E and V can be evaluated from knowledge of the initial conditions in the vessel. The total energy E is from the chemical energy available in the initial unburned mixture and the total volume V is the volume of the vessel (0.1853 cm^3 for the spherical and .1862 cm^3 for the cylindrical vessel). Therefore, the unknowns in these equations are the mass fraction burned,

the specific internal energy, and the specific volume of the burned gas. The specific internal energy and volume are both functions of the burned gas temperature, therefore, the two conservation equations have only two unknowns and can be solved.

The burned gases are modelled as a spherical region of gas (which burned at the first time step) surrounded by shells of burned gases which burned at later time steps. Each time-data point that is analyzed is considered a time step and therefore produces a shell of burned gas in the model. As time progresses in the experiment and pressure increases in the vessel, the already burned gases as well as the unburned gases continue to undergo a compression process produced by the ongoing combustion. This effect creates a temperature gradient in the burned gas core. The modelling account accounts for this effect by tracking the temperature of each burned gas shell and evaluating the temperature rise as an isentropic compression process. Gases in each shell are assumed to have uniform properties and to be in frozen chemical equilibrium. In this study the burned gas is allowed to have temperature gradients where in previous work a lumped method was used and the burned gas was assumed to be at an average temperature.

The two conservation equations can now be solved by using the two dimensional Newton-Raphson method. For this method the two equations are rewritten by:

$$\frac{V}{m}+\frac{A\delta}{m}=\sum_{i=0}^{n-1}v_{bi}x_i+v_{bn}x_n+(1-\sum_{i=0}^{n-1}x_i-x_n)v_u \tag{17}$$

$$\frac{E}{m}-\frac{Q}{m}=\sum_{i=0}^{n-1}e_{bi}x_i+e_{bn}x_n+(1-\sum_{i=0}^{n-1}x_i-x_n)e_u \tag{18}$$

In the equations above, the Newton-Raphson method described in APPENDIX 1 is used to solve for the properties of the nth shell x_n, e_{bn} and v_{bn} where e_{bn} and v_{bn} are functions of the temperature of the nth shell. The nth shell is last shell that has been consumed by the combustion process up to the time step in consideration. For example, in the first time step for n = 1 (spherical gas for this case) the summations sum to 0.0 because $x_o = 0.0$ and the two equations are solved for x_1, e_{b1}, v_{b1}. In the next time step n = 2 (first shell) e_{b1} and v_{b1} are reevaluated to account for the compression

due to burning of the first shell and the equations (17,18) are solved for x_2, e_{b2}, v_{b2}. This procedure is followed until the last time step, which is the time of maximum pressure in the bomb. The burned gas properties are calculated using STANJAN, a chemical equilibrium program that given temperature and pressure, calculates all the thermodynamic properties of the mixture at chemical equilibrium conditions (combustion products at the given temperature and pressure condition). The specific energy and volume of the inner shells (all shells up to the n-1 shell) are re-evaluated at temperatures that are adjusted to account for the compression from the nth shell. The temperatures are adjusted using an isentropic relation (equation 19) from the pressure at the previous time step (P_1), to the pressure at the time step being analyzed (P_2).

$$T_2 = T_1\left(\frac{P_2}{P_1}\right)^{\frac{\gamma_b - 1}{\gamma_b}} \tag{19}$$

Here γ_b is evaluated using STANJAN at temperature T_1, (the temperature at the previous time step) and it is assumed constant until T_2 because of the small variation in pressures (P_1 to P_2), which only alter the temperature and γ_b by a small amount.

By solving these two equations (17, 18) for the whole combustion process, the mass fraction of the burned gas and its numerical derivative versus time can be found. The derivative of the mass fraction burned is calculated by fitting a parabola to three consecutive points and differentiating to find the slope of the middle point, each point is used only once to avoid amplification of any possible errors. The mass burning rate MBR is simply evaluated by

$$MBR = m\,\dot{x} \tag{20}$$

The rate of mass fraction burned can be used to calculate the laminar burning speed when the proper conditions are present: non-stretched and non-cellular flames.

Equations 6 – 8 are used to calculate laminar burning speed.

$$S_u = mv_u \dot{x} / A_f \tag{6}$$

Where:

$\dot{x}$ = rate of mass fraction burned

A_f = the area of the flame = $4\pi R_f^2$ (7)

and, R_f, is the radius of the flame front:

$$R_f = \left(3V_b / 4\pi\right)^{1/3} \tag{8}$$

This is calculated from the volume of the burned gas:

$$V_b = xv_b m \tag{9}$$

5.0 RESULTS

5.1 Syngas Oxygen Helium

A large number of experiments have been performed at high pressure and temperature to measure the MBR and onset of auto-ignition for a wide range of syngas mixtures composed of hydrogen (H_2) and carbon monoxide (CO), a listing of the runs is found on Table 1. The percentages of H_2 in the mixture, defined as α, was varied in the following amounts 5%, 10% and 25% to best characterize the likely potential concentrations of H_2 available in typical syngas, especially when produced by biomass gasification. The syngas was combusted at fuel air equivalence ratios of 0.6, 1.0, 2.0, and 3.0 in a lower thermal capacity "air" 21%O_2-79%He. The purpose of using O_2-He as the air equivalent oxidizer is to achieve higher combustion temperatures. By substituting the nitrogen typically found in air with another inert gas such as helium, the total heat capacity of the mixture is reduced, therefore for the same heat of combustion the final temperature of the mixture is higher. All of the conditions described above were tested at an initial temperature of 400K for Stoichiometric conditions and initial pressure 2 atm runs. To compare and validate some of the results of this study with data in the literature, experiments were also performed at an initial temperature of 298K with air and with oxygen-helium "air" as the oxidizer, these experiments were performed at stoichiometric conditions, which is typically a point of interest in the combustion community. For syngas in oxygen-helium "air" the dependencies with respect to temperature and pressure were thoroughly investigated. The initial pressure conditions were set to 2, 5, 10 atm and initial temperatures to 298, 400, and 450K with a few runs at 480K for auto-ignition testing. The resulting trends for MBR are plotted against pressure and temperature of the unburned gases. It was found that for initial pressure higher than 2 atm the flames quickly become cellular and therefore a smooth flame area, and hence laminar burning speed (LBS) cannot be calculated. Laminar burning speed was calculated and compared to the literature for the a few of the low initial pressure runs were the flame was visually inspected using the cylindrical vessel and non-cellular range of the data used for the calculations. Unfortunately, within the testing capability of this facility no auto-ignition was detected for all the mixtures of syngas tested. Therefore, the only conclusion that can

be made, is that the auto-ignition temperature for the syngas mixtures tested is higher than the maximum temperature achieved in this study. The temperatures in the experiments of this study peaked at ~ 800K for α = 5%, this temperature is considerably lower than the auto-ignition temperatures for α=5% reported by Apurba k. Das et al. [27] at Case Western University.

Range of Testing: Syngas Helium Air			
Phi	α (%)	Initial Pressure (atm)	Initial Temperature (K)
1.0	5	2 -12	400 - 500
1.0	10	2 - 10	400 - 450
1.0	25	2 - 10	400 - 450
0.6	5	2 - 5	400 - 450
0.6	10	2 - 5	400 - 450
0.6	25	2 - 5	400
2	5	5 -12	400 - 500
2	10	5	400
2	25	5	400
3	5	5	400
3	10	5	400
3	25	5	400

Table 1: Range of Testing for Syngas Helium

5.2 Syngas-Air Laminar Burning Speed

The pressure rise from numerous syngas combustion events in a constant volume vessel was measured. Only the measured data for the initial part of the experiment where the flame front is smooth and non-cellular was considered for the analysis and calculation of LBS. The flame front

was visually inspected using the cylindrical vessel for the on-set of cellularity and experimental data beyond this point is neglected for the purpose of evaluating LBS. Furthermore, when cellularity begins the LBS deviates from a linear function of flame radius, this is confirmed in the cylindrical vessel by visual inspection. The deviation of LBS from a linear function of flame radius is used to crop the data collected from the spherical vessel where visual inspection is not possible. For syngas-air and most other combustible mixtures, the flame front is burdened with high flame stretch front from the start of the combustion up to a flame radius of approximately 4 cm, this is also commonly found in the literature and calculated by other [21]. The data in this initial region and therefore this part of the measurement is not included in the LBS calculation.

Figure 25 shows the syngas-air pressure data for Φ =1.0 and initial pressure of 2 atm, before the preprocessed to eliminate the initial "stretched" portion and the end "cellular" portion of the flame, leaving data suitable for LBS calculation.

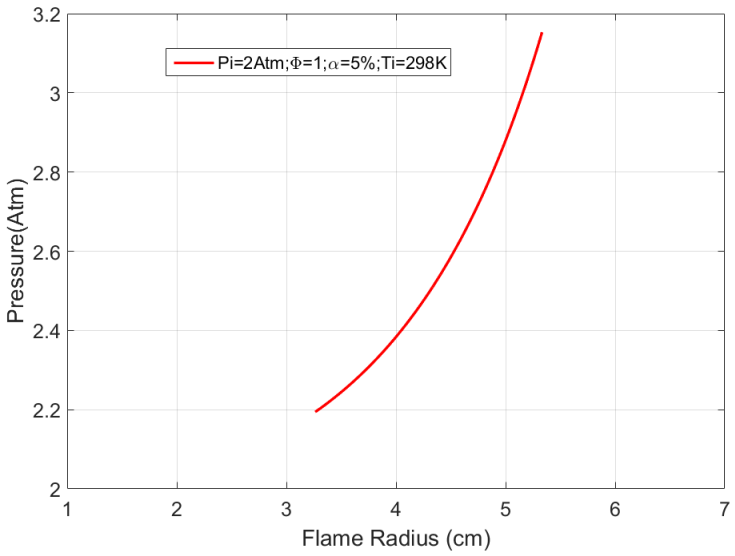

Figure 25:Pressure vs. time typical for Syngas-air experiment

As previously reported flame stretch and cellularity effect the validity of the measurement and model [28]. Laminar burning speed is by definition non-stretched and therefore the stretch that can effect the calculations are avoided. Stretch can be calculated by the following equation:

$\alpha = \frac{1}{A}\frac{dA}{dt} = \frac{2}{r}\frac{dr}{dt}$ and the acceptable threshold among the scientific community resulting from various studies is α < 100 1/sec do not have a strong impact on LBV. In Appendix 2 a more detailed analysis of the typical stretch found in syngas flame demonstrates that for flame radius > 4 cm the flame stretch is ignorable. A similar result will be shown in the following figure by visual inspection of the plot of LBS vs. flame radius. In Figure 26, the region below a flame radius of approximately 3.75 cm shows a nonphysical behavior for the LBS, in fact only in the region between ~ 4 and 5.5 cm can LBS be accurately calculated. Beyond a flame radius of 5.5 cm, the flame front becomes cellular, as indicated by the high speed images (Figure 28), and at that point LBS starts to deviate from a linear function of flame radius.

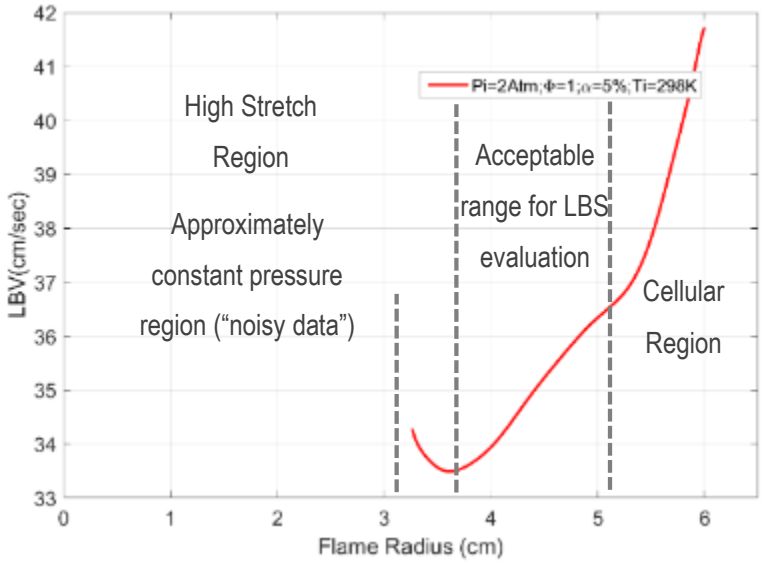

Figure 26: Syngas-Air LBS vs. flame radius, indicating stretch and cellularity effects

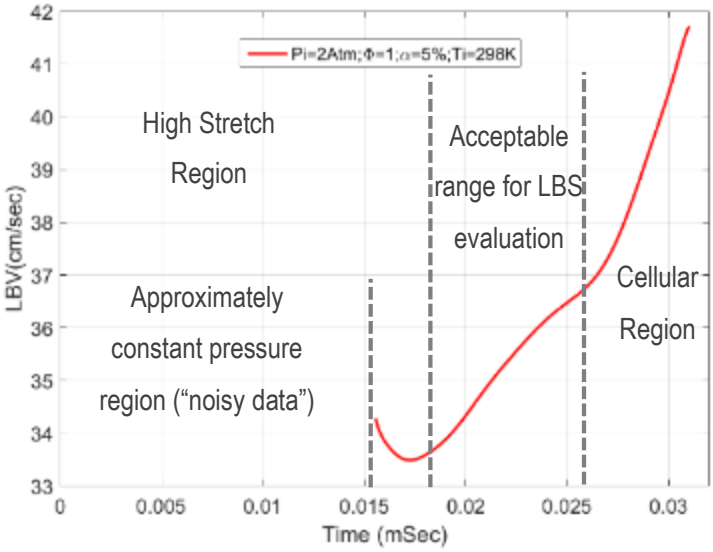

Figure 27: Syngas-Air LBS vs. time, indicating stretch and cellularity effects

Syngas –Air α=5%, Ti=298K; Pi=2 atm; Φ=1;

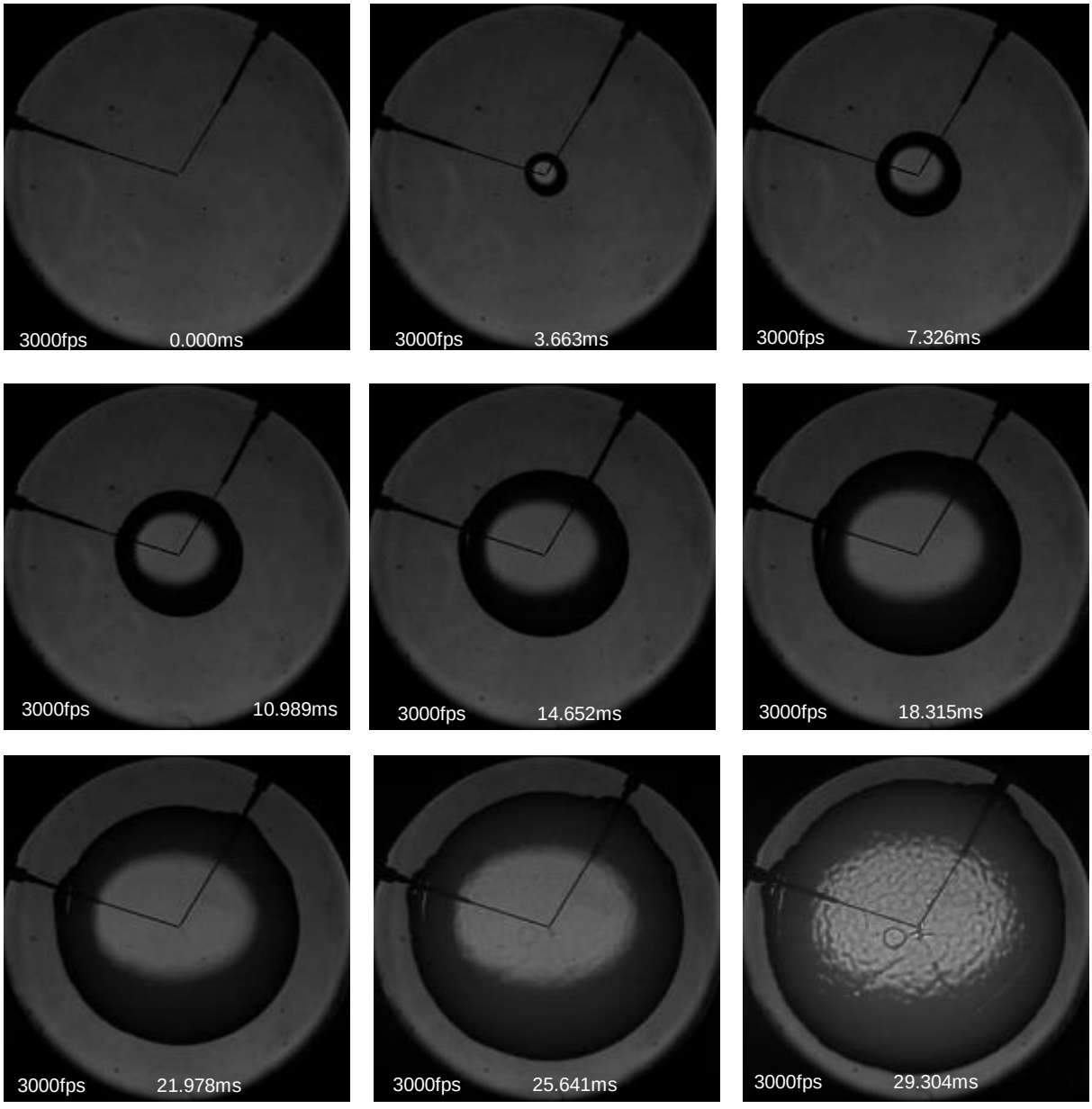

Figure 28: High speed images of flame front for Syngas Φ=1.0,α=5%, initial pressure 2Atm

Figure 27 and Figure 28 indicate the effects of high stretch and cellularity on LBV, cellularity is visually confirmed by matching the point on the graph were LBS deviates from linearity to the high

speed images. Both techniques produce the same result, the on-set of cellularity occurs at approximately 26ms in the high speed images. A starting point for selecting the non-stretched portion of the measurements is to select data for pressure values >10% of the initial pressure. This is typically found to indicate a radius >4cm for most syngas-air experiments.

Figure 29 and Figure 30 show the portion of the pressure data that are used in the LBS analysis and evaluation.

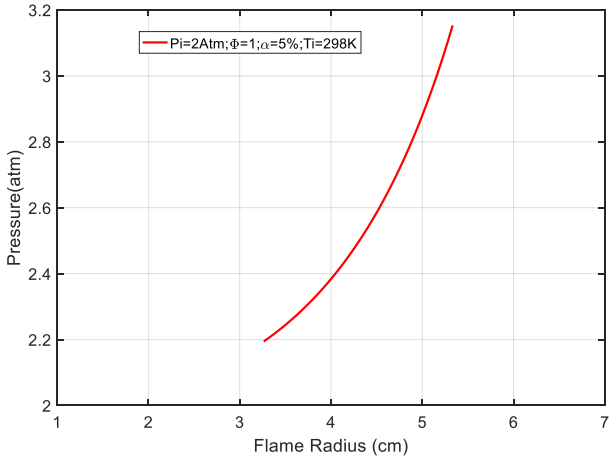

Figure 29: Pressure vs. flame radius scrubbed for LBS calculations

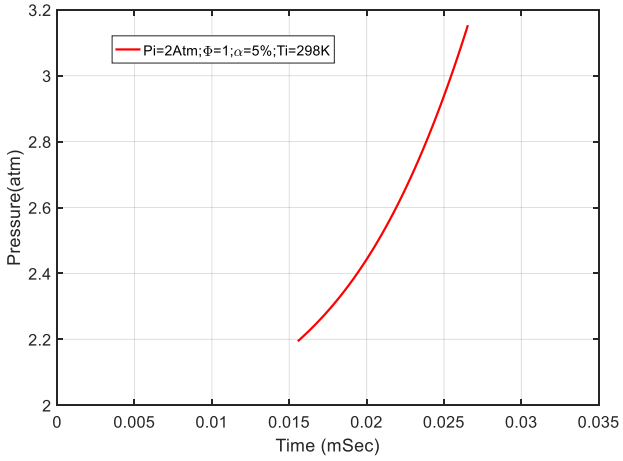

Figure 30:Pressure vs. time scrubbed for LBS calculations

This section so far has demonstrated the method of processing the experimental data to select the portion appropriate for evaluating LBS based on the model's assumptions. However, to adequately map the LBS behavior across the range on temperatures, pressures, stoichiometry and any other desired parameters many data runs are required. For syngas air mixtures, several experimental runs were chosen for evaluation LBS and comparison to data reported in the literature. The LBS results of this study have been compared to measurements at equivalent conditions. Good agreement between this study and others [29] was found and indicated in Figure 31, Figure 32 and Figure 33.

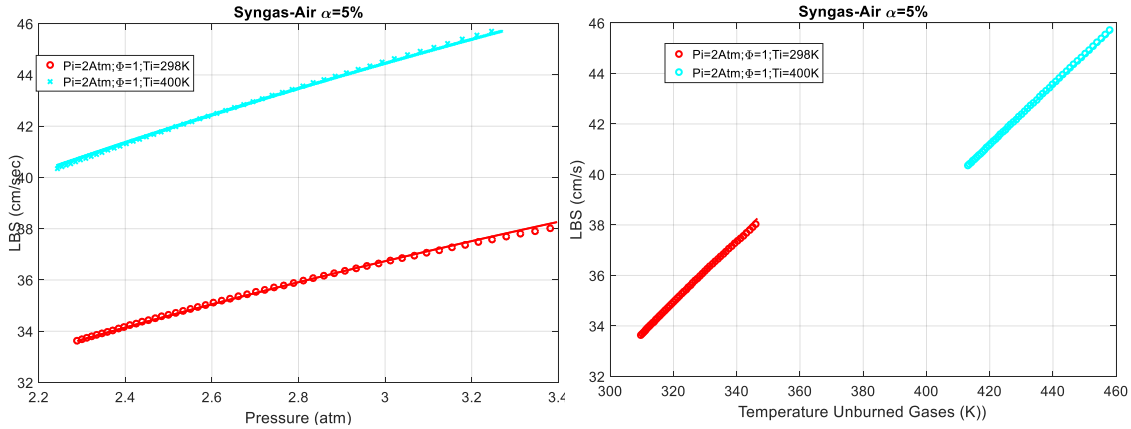

Figure 31: LBS for Stoichiometric Syngas-air α=5%, along pressure and temperature isentropes

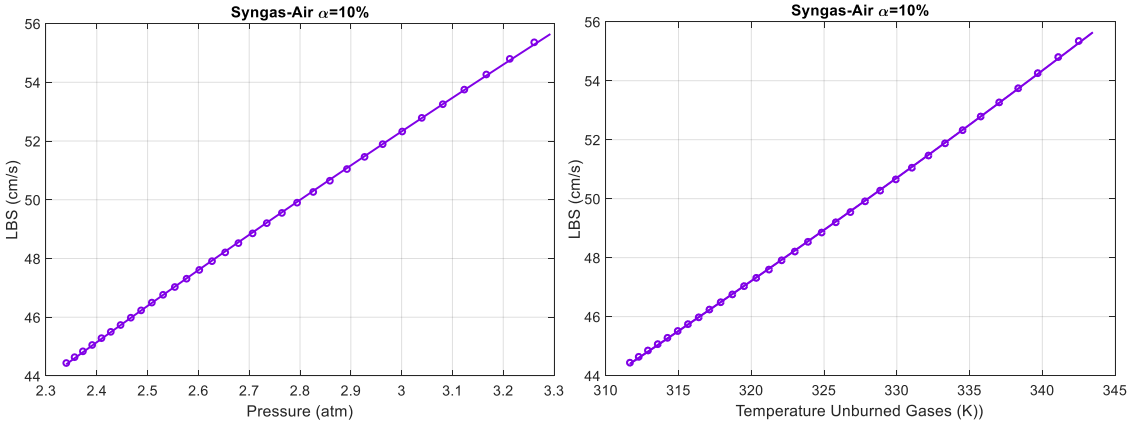

Figure 32: LBS for Stoichiometric Syngas-air at α=10%, along pressure and temperature isentropes

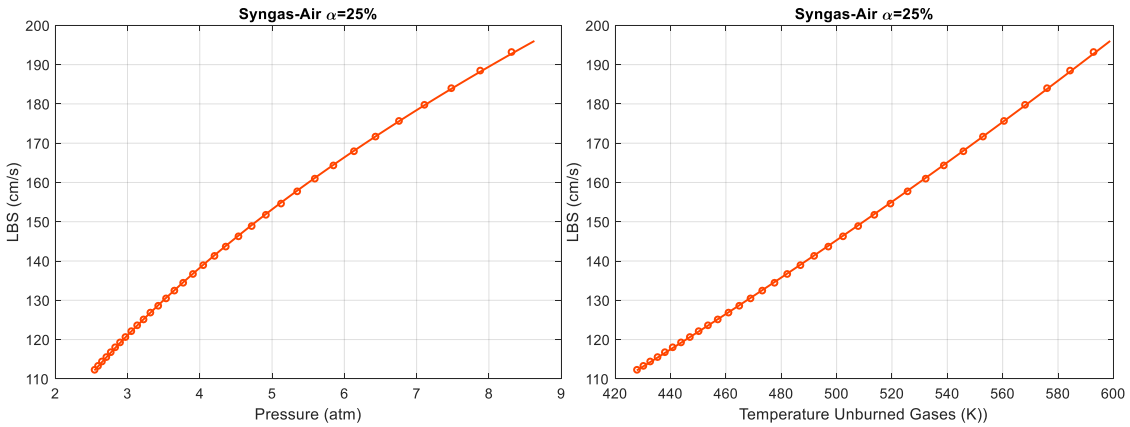

Figure 33:LBS for Stoichiometric Syngas-air at α=25%, along pressure and temperature isentropes

A proposed correlation for LBS for Syngas-air at Φ=1.0 is given in the form:

$$S_u = S_{u0}\left[\frac{T_u}{T_{u0}}\right]^{\lambda}\left[\frac{P}{P_0}\right]^{\beta} \qquad (21)$$

Where T_u and P represent the unburned gas temperature and pressure of the system, and T_{u0}, P_{u0}, and S_{u0}, represent the temperature, pressure and LBS respectively at reference conditions: 298K, 1.0 atm. The coefficients of the fits are listed in Table 2 for different values of α.

Syngas-Air	S_{u0} (cm/sec)	λ	β	Average fit error (%)	Valid Range	
α=5 %	29.2	.6528	.1417	.002	2-3.5 atm	300-460 K
α=10 %	40.0	2.32	.0005	.044	2-3.5 atm	300-350 K
α=25 %	61.0	1.74	-.0220	.005	2-9 atm	400-600 K

Table 2: Coefficients and Error of correlation for Syngas-Air LBS

Both the calculated error of the correlations and fit shown in the figures (Figure 35,Figure 36,Figure 37) demonstrate excellent agreement with the measured data and with data by Askari O. [29].

5.3 Syngas-O2-He

As previously mentioned, a common technique to increase the pressure and temperature measurement range of LBS is to replace the nitrogen typically found in air with a lower specific heat inert gas such as helium. For syngas in O_2-3.76He at α=5,10,25% initial pressure, temperatures and stoichiometry have been varied and LBS is reported in this study. Unfortunately, no comparative data was found in the literature for the extended range of high temperature and pressure that was tested in this study.

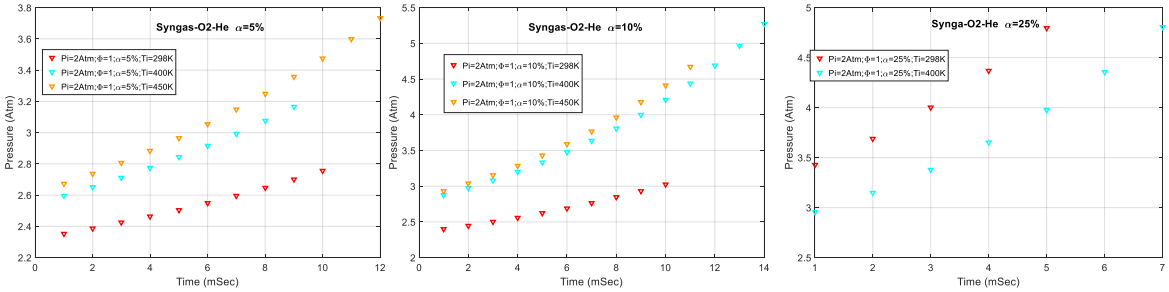

Figure 34: Processed Pressure rise of Syngas (α= 5-10-25%), Φ=1.0, initial pressure 2 atm.

The pressure data collected for syngas-O2-He mixtures at low initial pressure was processed using the same techniques described in section 5.2 to cut out the range of data where high stretch and cellularity are present in the flame front. The processed pressure data is shown on Figure 34 for syngas at α=5%,10%,15%. Laminar burning speed was evaluated for these low initial pressure runs and fitted to the following correlation. The measured data is plotted in the following Figure 35 as circle markers and the proposed correlation as solid line.

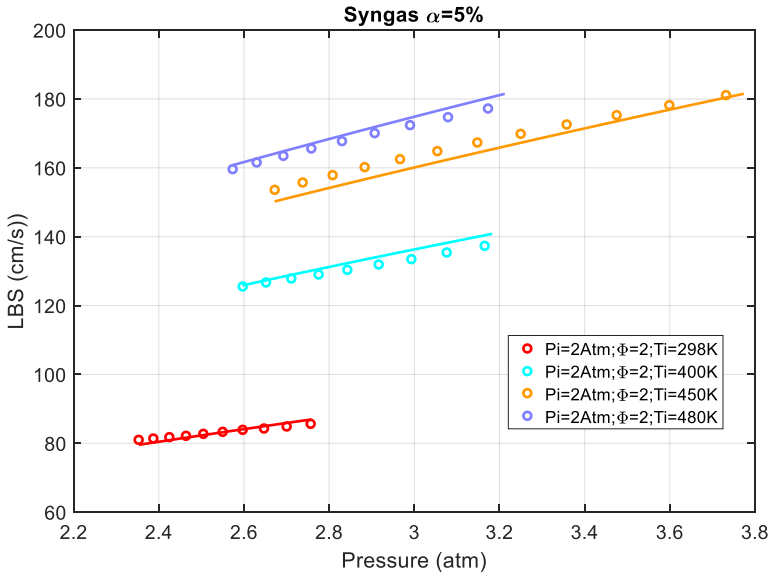

Figure 35: Laminar Burning Speed of Syngas with α= 5%

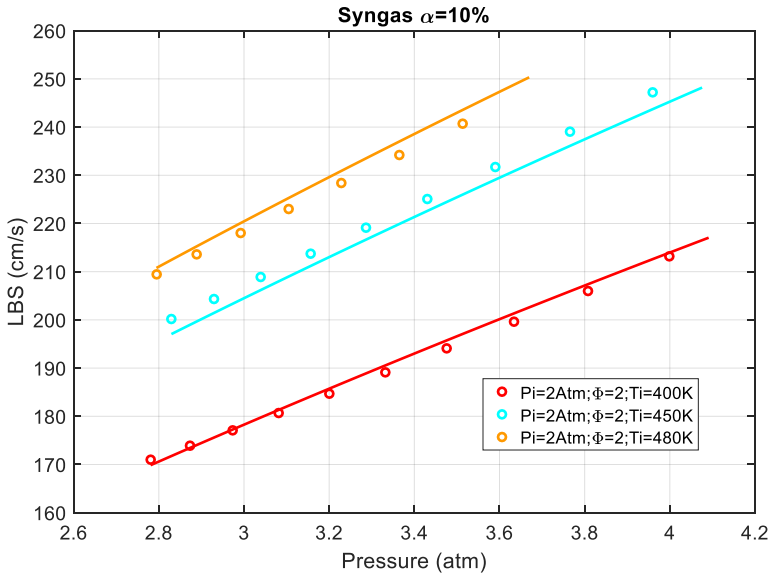

Figure 36: Laminar Burning Speed of Syngas with α= 10%

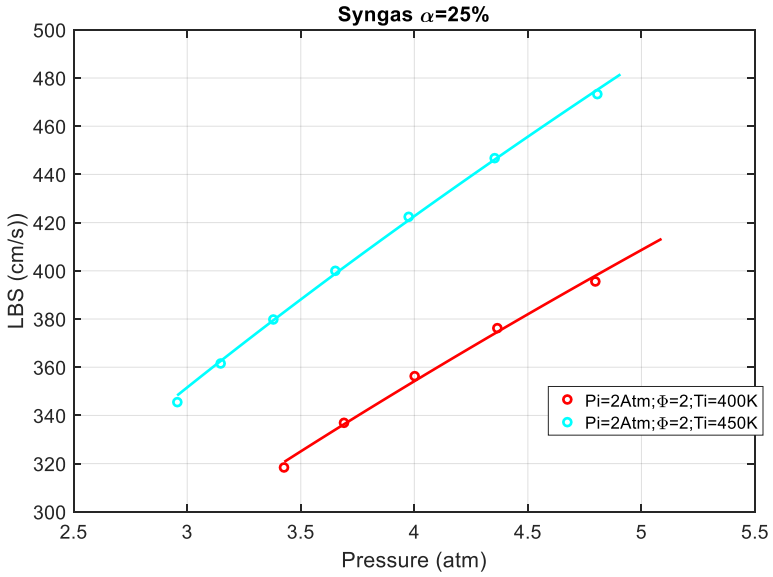

Figure 37: Laminar Burning Speed of Syngas with α=25%

The form of proposed correlation for LBS for syngas 21%O2-79%He at Φ=1.0 is:

$$S_u = S_{u0}\left[\frac{T_u}{T_{u0}}\right]^{\lambda}\left[\frac{P}{P_0}\right]^{\beta} \quad (21)$$

Where T_u and P represent the unburned gas temperature and pressure of the system, and T_{u0}, P_{u0}, and S_{u0}, represent the temperature, pressure and LBS respectively at reference conditions: 298K, 1.0 atm. The coefficients of the fits are listed in Table 3 for different values of α.

Syngas in O2-He with	**S_{u0} (cm/sec)**	**λ**	**β**	**Average fit error (%)**
α=5 %	68.23	1.375	.091	.050%
α=10 %	82.5	1.17	.24	.010%
α=25 %	131.9	1.518	.136	.001%
Valid for T_u 298- 550K Pressure 2-4atm				

Table 3: Coefficients and Error of correlation for Syngas-O2-He LBS

Both the calculated error of the correlations and fit shown in Figure 35, Figure 36, and Figure 37 demonstrate excellent agreement with the measured data.

5.4 Syngas mass burning rate

LBS cannot be evaluated in cellular flames unless further knowledge regarding the shape and area of the cellular flame becomes available, however, mass burning rate can be measured and evaluated using the same model and assumptions. For the same experimental runs the mass burning rate can be evaluated for almost the entire range of measured pressure without cropping any of the data due to cellularity effects. Many experimental data runs have been analyzed and the data is summarized in the figures and tables below:

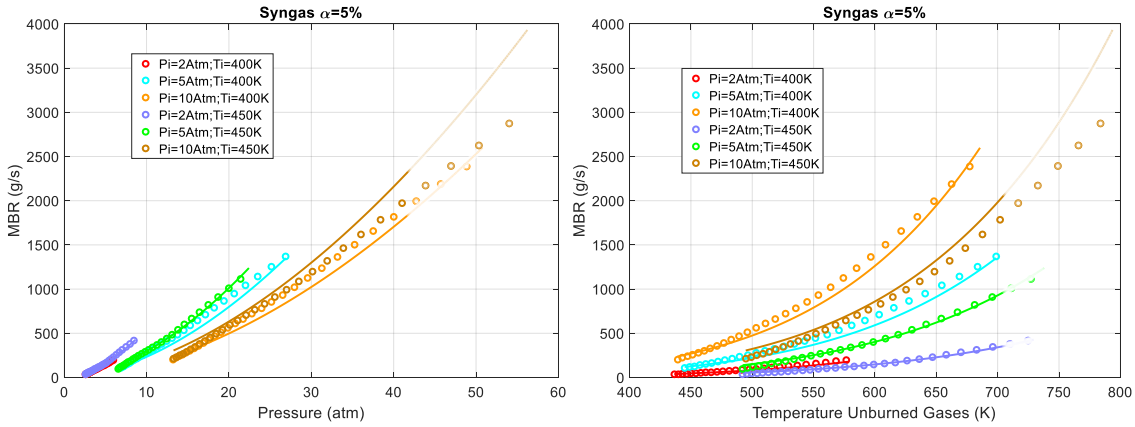

Figure 38: MBR of Syngas with α=5% ϕ =1.0 vs pressure and temperature

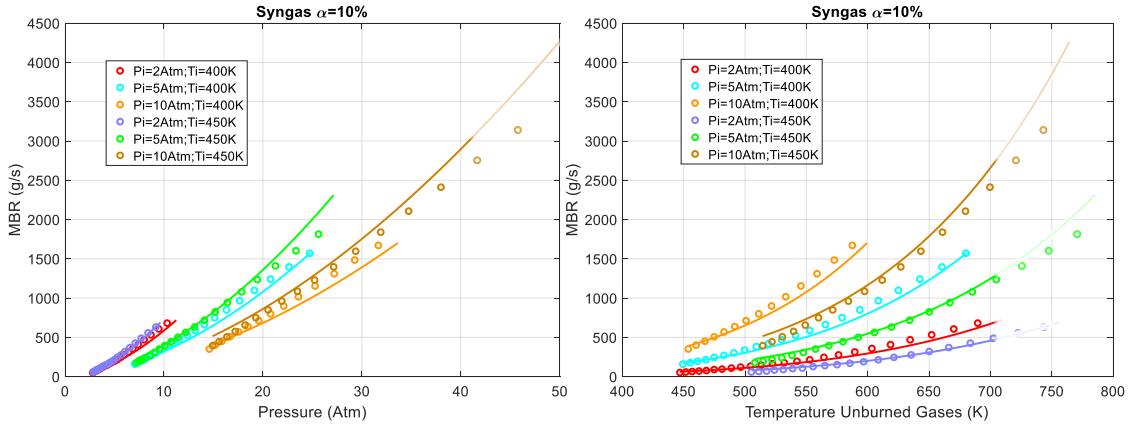

Figure 39: MBR of Syngas with α=10% ϕ=1.0 vs pressure and temperature

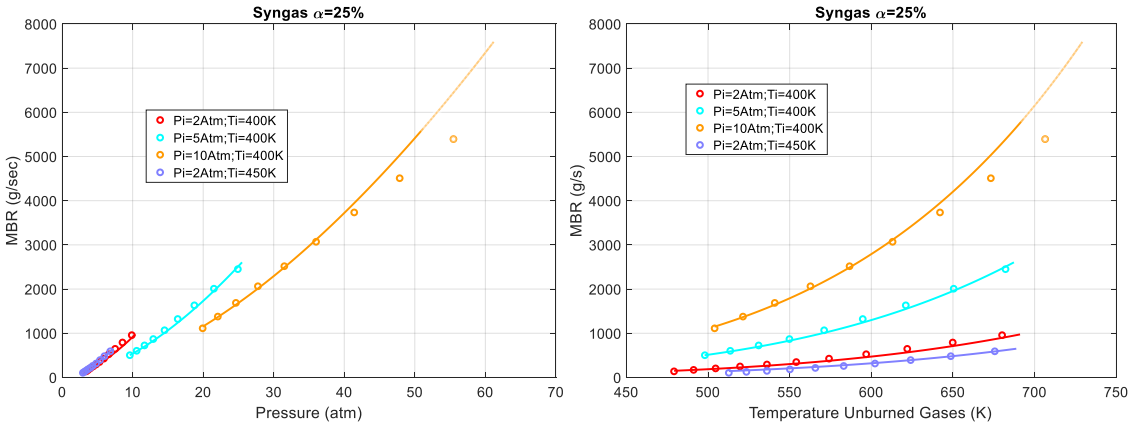

Figure 40: MBR of Syngas with α=25% ϕ=1.0 vs pressure and temperature

The MBR data was fitted to a similar form of proposed correlation for LBS for each concentration of H_2 in the mixture (α=5,10,25%):

$$MBR = MBR_0 \left[\frac{T_u}{T_{u0}}\right]^{\lambda} \left[\frac{P}{P_0}\right]^{\beta} \quad (22)$$

Where T_u and P represent the unburned gas temperature and pressure of the system, and T_{u0}, P_{u0}, and S_{u0}, represent the temperature, pressure and LBS respectively at reference conditions: 298K, 1.0 atm. The coefficients of the fits are listed in Table 4 for different values of α.

Syngas in O2-He with	MBR_0 (g/sec)	λ	β	Average fit error (%)	Max Error (%)	Valid Range		
						ϕ	T_u (K)	P (atm)
α=5 %	6.33	2.06	1.09	5.53%	10.0% @ 700K, 41Atm	1.0	400-700	2 - 41
α=10 %	9.04	2.00	1.09	5.12%	10.5% @700K, 40Atm	1.0	400-700	2 – 40
α=25 %	16.78	1.76	1.10	8.74%	13.5% @690K, 51Atm	1.0	400-690	2 - 51

Table 4: Coefficients and Error of Correlation for Syngas-O2-He MBR

MBR measurements were also taken at varying fuel air equivalence ratios and the data was fitted to a similar form of proposed correlation for LBS for each concentration of H_2 in the mixture (α=5,10,25%):

$$MBR = MBR_0(1 + a(\phi - 1) + b(\phi - 1)^2)\left[\frac{T_u}{T_{u0}}\right]^{\lambda}\left[\frac{P}{P_0}\right]^{\beta} \quad (23)$$

Where T_u and P represent the unburned gas temperature and pressure of the system, and T_{u0}, P_{u0}, and S_{u0}, represent the temperature, pressure and LBS respectively at reference conditions: 298K, 1.0 atm. The measured and fitted data is shown on the following figures for α=5% and 10%, the coefficients of the fit are tabulated on Table 5.

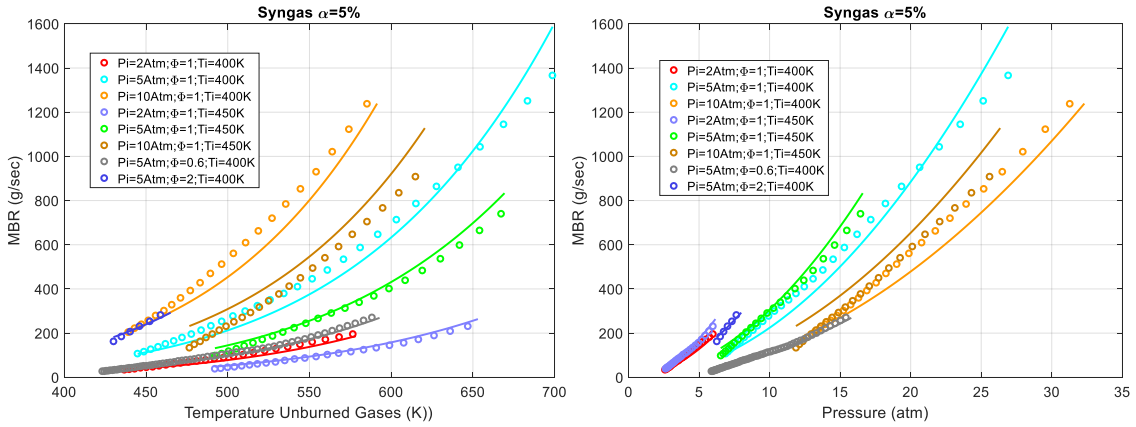

Figure 41: MBR of Syngas with α= 5% vs pressure and temperature

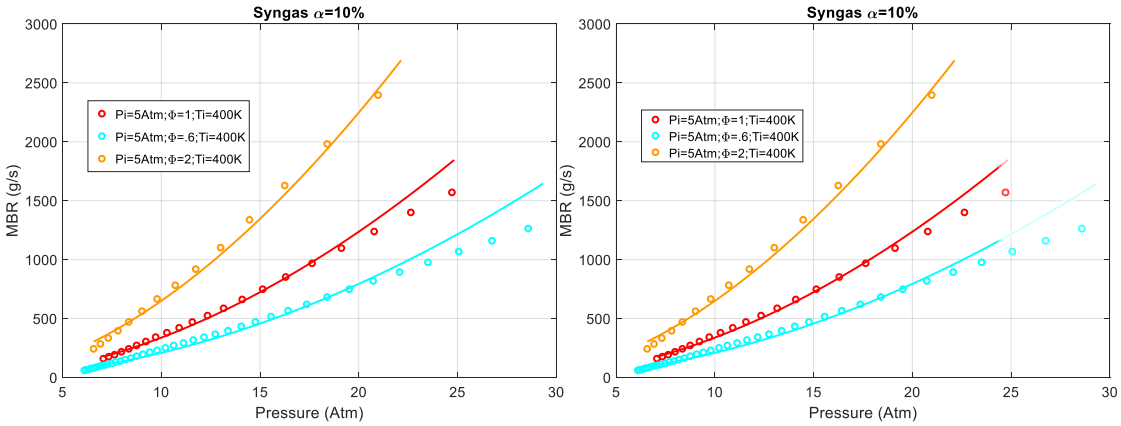

Figure 42: MBR of Syngas with α= 10% vs pressure and temperature

Syngas -O2-He	MBR_0 (g/sec)	a	b	λ	β	Average fit error (%)	Max Error (%)	Valid Range		
								ϕ	T_u (K)	P (atm)
α=5 %	4.39	1.75	-.173	2.68	1.09	.02%	12.0% @ 680K, 25Atm	0.6-2.0	400-680	2 - 25
α=10 %	18.1	1.02	.0187	5.915	-.082	2.54%	13% @680K, 24Atm	0.6-2.0	400-680	2 – 24

Table 5: Coefficients and error for Syngas-O2-He MBR at Varying Stoichiometry

5.5 Heptane auto-ignition

Heptane is a commonly used fuel in studies involving auto-ignition due to its low propensity to auto-ignite [30]. In this study, heptane was used to validate the experimental apparatus and technique for measuring the onset of auto-ignition. Other techniques commonly used to measure auto-ignition involve either a shock tube or rapid compression machine [31]. In both methods a rapid increase in pressure up to a fixed value is forced on a combustible mixture then the time for the mixture achieve a noticeable temperature increase is measured (based on pressure measurements) and reported as the auto-ignition delay [32]. The temperature increase that is typically detected is approximately 1000K surely resulting from a combustion process. The time a mixture can reside at a certain temperature and pressure condition before the onset of auto-ignition is defined as the ignition delay, in this study the temperature and pressure conditions that instantaneously produce auto-ignition are measured and reported as the onset of auto-ignition. Measurements of stoichiometric heptane auto-ignition in 21%O_2-79%He were performed at initial pressures of 5,9, and 10Atm with 450, 475 and 450K initial temperature respectively, the results are shown in Figure 43, Figure 44 and Figure 45.

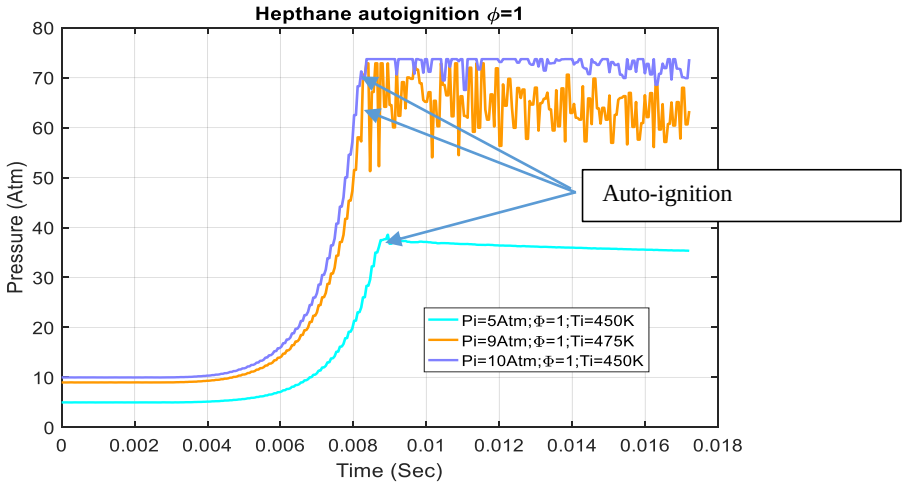

Figure 43: Stoichiometric Heptane auto-ignition pressure traces

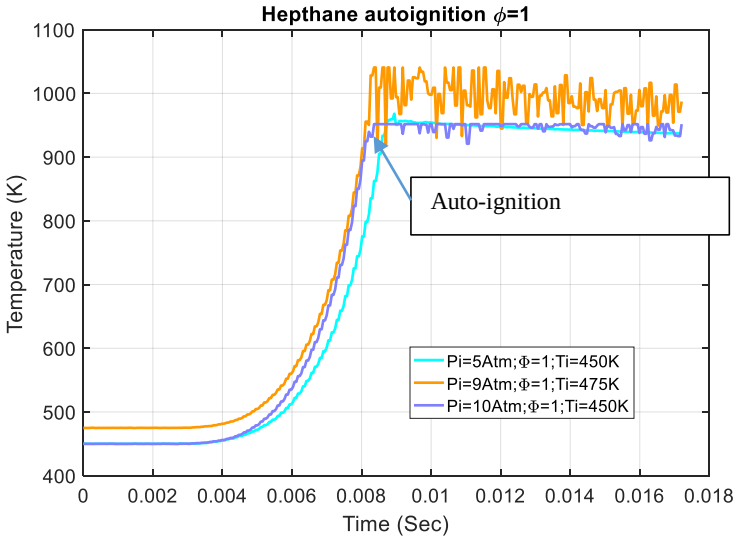

Figure 44: Stoichiometric Heptane auto-ignition temperature trace

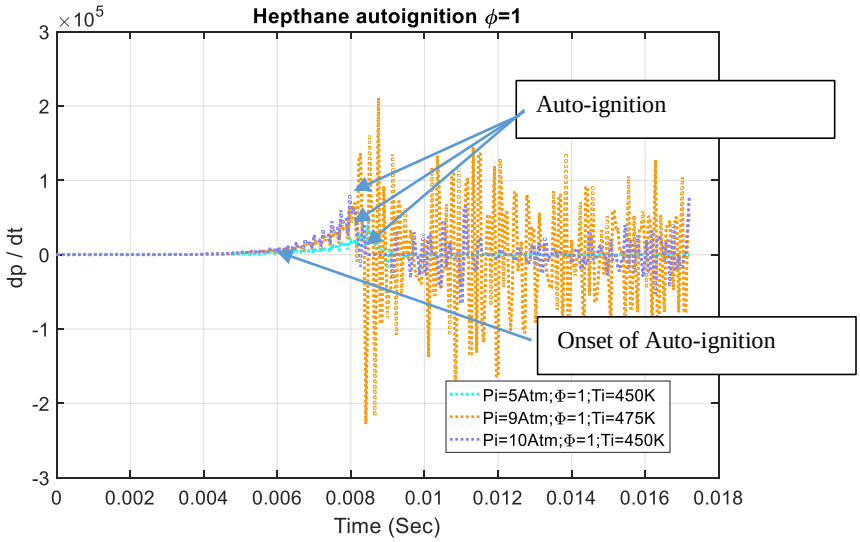

Figure 45: Stoichiometric Heptane auto-ignition pressure rate (dp/dt)

These experimental runs produced auto-ignition conditions at different pressures and temperatures, indicating, as expected, that the auto-ignition characteristics are a strong function of the temperature of the unburned gases. Both the temperature and pressure dependencies are positive, as either

temperature or pressure are increased, the propensity of auto-ignition increases. To detect the onset of auto-ignition the derivative of the measured pressure dp/dt can be evaluated and used as a non-subjective method. The measured pressure signal begins to oscillate once auto-ignition occurs due the shock waves bouncing around in the combustion vessel. The derivative with respect to time of the pressure signal will oscillate very aggressively between positive and negative values once auto-ignition occurs thus providing a very convenient method to detect the on-set of auto-ignition. The unburned gas conditions at the onset of auto-ignition are measured to be in the range of 506-526K for the three conditions tested this is consistent with the minimum auto-ignition temperature reported in the literature for heptane [33].

Auto-ignition for stoichiometric Heptane at small ignition delay <<1ms		
Experiment	Temperature of unburned gases	Pressure
Run1: Ti = 450K, Pi=5 atm	953 K	37.5 atm
Run2: Ti = 475K, Pi=9 atm	944 K	57 atm
Run1: Ti = 450K, Pi=10 atm	934 K	71 atm

Table 6: Auto-ignition conditions for stoichiometric Heptane at ~1.0 ms ignition delay

To compare the results of this study to published data, ignition delays of less than 1.0 ms are considered. The unburned gas conditions ~1.0ms prior to the detection of auto-ignition in this study, are compared to values of the unburned gas conditions, reported at an ignition delay of 1.0 ms. Higher speed pressure data collection may enable shorter ignition delays to be resolved, currently the pressure data is collected at the maximum rate (10kHz).

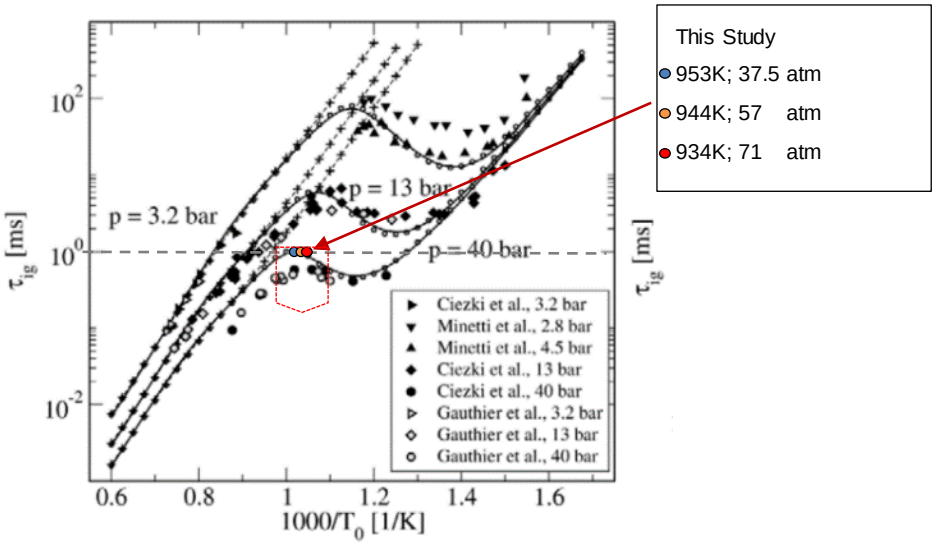

Figure 46: Comparison of measured Heptane auto-ignition [33]

5.6 GTL auto-ignition

As previously discussed, synthetic fuels produced by the Fisher-Tropsch method have become increasingly popular as substitutes to the conventional hydrocarbon fuels such as diesel, gasoline, and jet fuels [34]. The GTL (S8) developed by the Syntroleum Corporation was designed to be a direct replacement (surrogate) of Jet-A fuel, the most commonly used aviation fuel. In this study the propensity of S8 to auto ignite and the conditions that produce the onset of auto-ignition was measured and analyzed for varying fuel air equivalence ratios and initial conditions. As previously discussed, the results of this study are compared to other measurements for very small ignitions delays <1ms as to compare results at approximately similar experimental conditions. The conditions measured by this study 1.0 ms prior to the completion of auto-ignition are compared to other studies. Measurements for the onset of auto-ignition of S8 at fuel air equivalence ratios of 0.8-1.2 and at initial conditions of 3,6,8.6,10,12 atm and 450K the results are shown in Figure 47 and Figure 55, along with the conditions that produce the onset of auto-ignition. The results of the technique previously described to systematically detect the onset conditions by differentiation of the pressure signal are show in Figure 49, Figure 52 and Figure 55, for all the conditions tested. It can be observed visually that the oscillatory pressure waves caused by auto-ignition are easily detected by this technique.

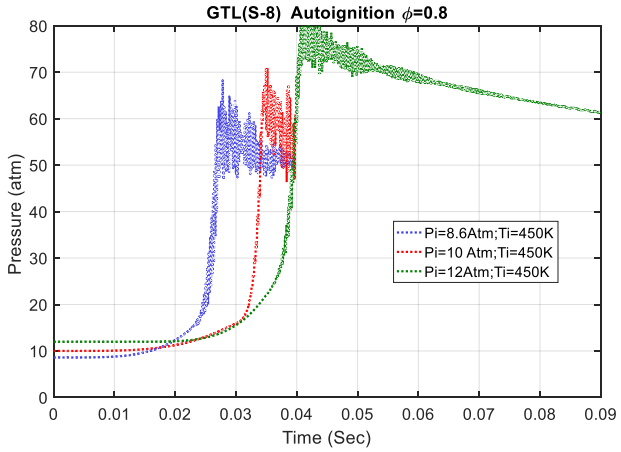

Figure 47: Pressure measurement and the onset of auto-ignition for S8 at Φ=0.8

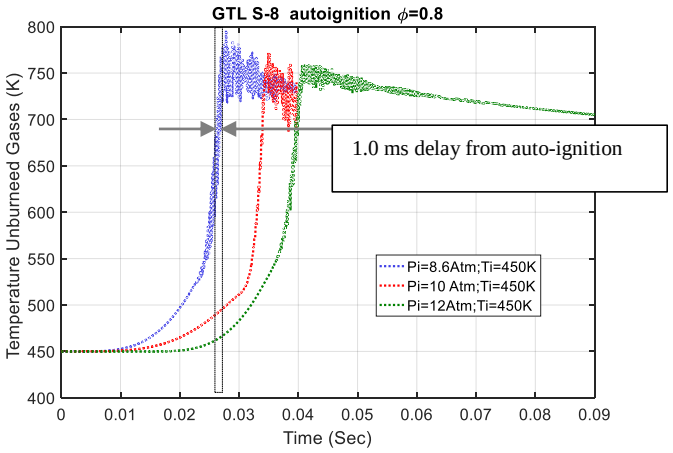

Figure 48: Temperature measurement and the onset of auto-ignition for S8 at Φ=0.8

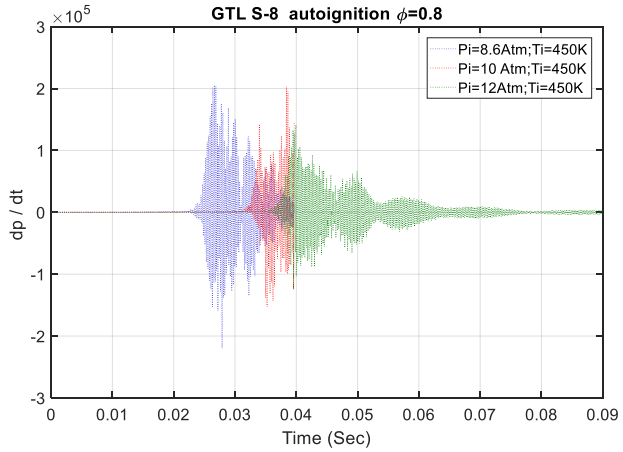

Figure 49: Pressure rate (dp/dt) for detecting the onset of auto-ignition for S8 at Φ=0.8

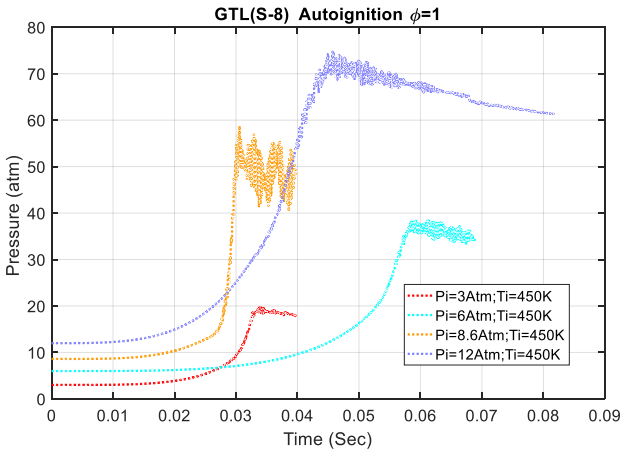

Figure 50:Pressure measurement and the onset of auto-ignition for S8 at Φ=1.0

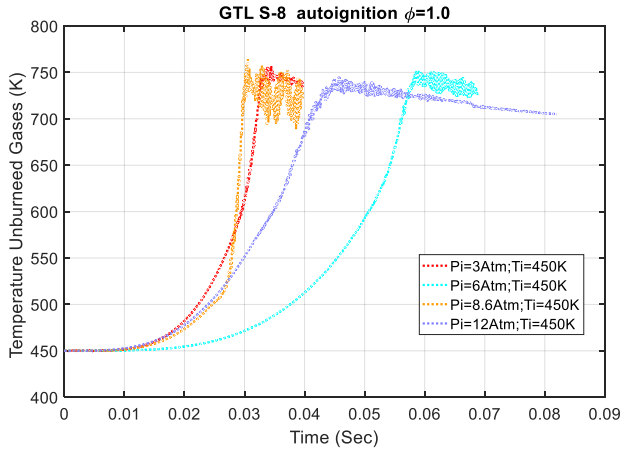

Figure 51:Temperature measurement and the onset of auto-ignition for S8 at Φ=1.0

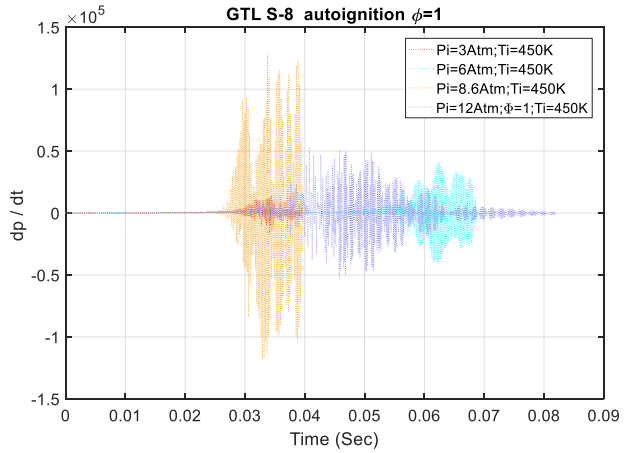

Figure 52: Pressure rate (dp/dt) for detecting the onset of auto-ignition for S8 at Φ=1.2

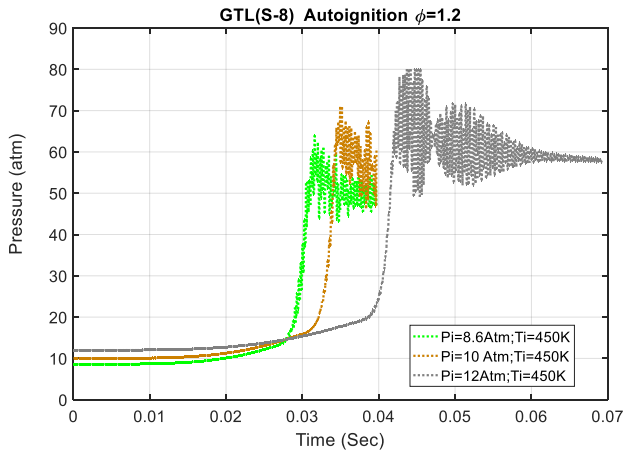

Figure 53:Pressure measurement and the onset of auto-ignition for S8 at Φ=1.2

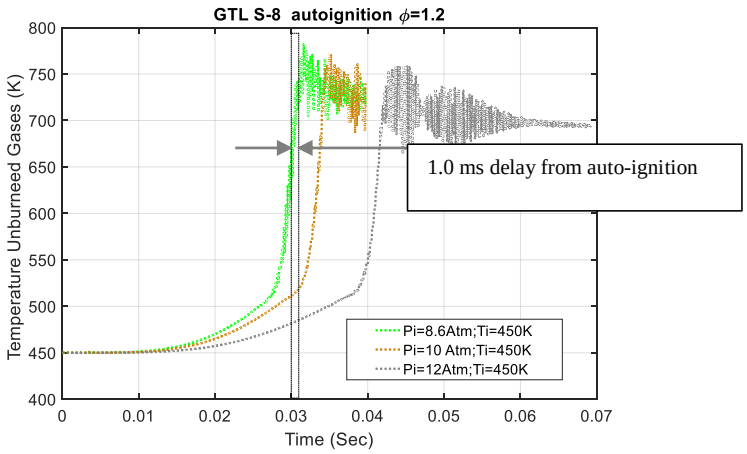

Figure 54:Temperature measurement and the onset of auto-ignition for S8 at Φ=1.2

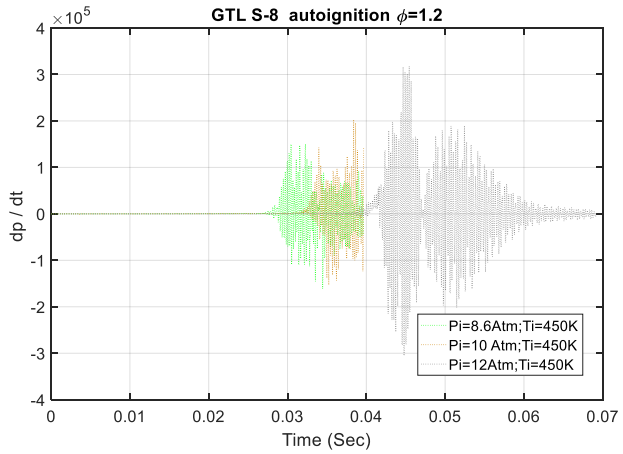

Figure 55: Pressure rate (dp/dt) for detecting the onset of auto-ignition for S8 at Φ=1.2

These experimental runs produced auto-ignition conditions at different pressure and only slightly different temperature, indicating, as expected, that the auto-ignition characteristics are a strong function of the temperature of the unburned gases. Both the temperature and pressure dependencies are positive, as either temperature or pressure are increased the propensity of auto-ignition increases. To detect the onset of auto-ignition the derivative of the measured pressure dp/dt can be evaluated and used as a non-subjective method. The measured pressure signal begins to oscillate

once auto-ignition occurs due the shock waves bouncing around in the combustion vessel. The derivative with respect to time of the pressure signal will oscillate very aggressively between positive and negative values once auto-ignition occurs thus providing a very convenient method to detect the on-set of auto-ignition. The unburned gas conditions at the onset of auto-ignition are tabulated below (Table 7), the average onset of auto-ignition temperature is 535K which compares well with result described as the "onset of reactivity" by Stephen Dooley et al. [35]

On-set of auto-ignition for stoichiometric S8 (GTL aviation surrogate)			
Experimental Initial Conditions	Fuel air equivalence Ratio	Temperature of unburned gases (K)	Pressure (atm)
Ti = 450K, Pi=8.6 atm	0.8	517	14.17
Ti = 450K, Pi=10 atm	0.8	524	17.24
Ti = 450K, Pi=12 atm	0.8	540	22.97
Ti = 440K, Pi=3 atm	1.0	553	6.87
Ti = 450K, Pi=6 atm	1.0	556	12.9
Ti = 450K, Pi=12 atm	1.0	559	26.3
Ti = 450K, Pi=8.6 atm	1.2	515	14.0
Ti = 450K, Pi=10 atm	1.2	523	17.24
Ti = 450K, Pi=12 atm	1.2	523	20.7
		Average = 535 K	

Table 7: Conditions at on-set of auto-ignition for GTL (S8)

To compare the results of this study to published data, ignition delays of approximately 1.0 ms are considered. The unburned gas conditions 1.0 ms prior to the detection of auto-ignition in this study, are compared to values of the unburned gas conditions, reported at an ignition delay of 1.0 ms. It should be noted that the data available in the literature is relatively coarse with respect to ignition delay and pressure. For ignitions delay shorter than 1.0 ms the data of this study agrees well with others [36], however longer ignition delays are not reasonable to compare since the unburned conditions may vary at rates of up to ~ 100 K/ ms. Higher speed pressure data collection may enable shorter ignition delays to be resolved, currently the pressure data is collected at the maximum rate (10kHz). Results of this study are compared to results from Kamal K. et al. [36] on

Figure 56 for ϕ=1.2 where the pressure dependency infers that the data in this study matched well. In Figure 57 the comparison is made at both ϕ=0.8 and 1.2.

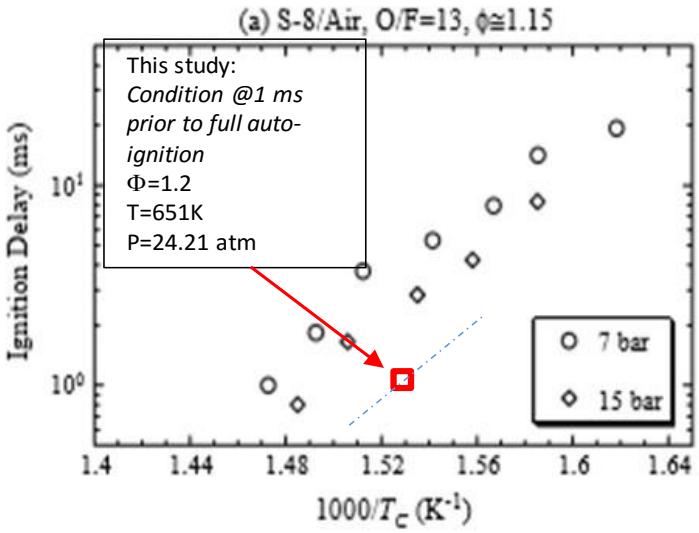

Figure 56: Ignition Delay at Φ=1.2, pressures 7 and 15 atm, chart from [36]

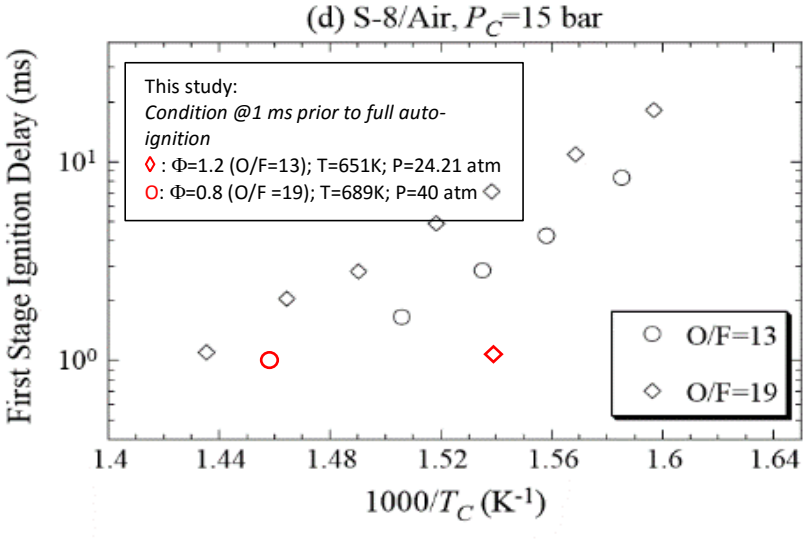

Figure 57: Ignition Delay at Φ=0.8 and 1.2, pressure 15 atm, chart from [36]

6.0 SUMMARY AND RECOMMENDATIONS

6.1 Summary

A state of the art combustion laboratory, first initiated by the author in 1997, has been developed at Northeastern University, with the help of many other researches over the past ~ 20 years. The facility is fully operational and has produced a tremendous amount of knowledge for the scientific combustion community especially in the areas of laminar burning speed, flame characterization and auto-ignition. This study summarized the experimental facility with all its newest updates and the modelling required to analyze the measured data to evaluate mass burning rate, laminar burning speed (under proper conditions) and onset of auto-ignition. In addition, new data was measured and reported for new and interesting new fuels: Syngas and GTL (S8) a synthetic aviation fuel surrogate.

For Syngas-air and Syngas-O_2-He the unburned gas conditions achieved at the end of combustion with the current capabilities of this facility did not produce auto-ignition result. The conditions achieve peaked at ~800K, this is consistent with both H_2 and CO having high auto-ignition thresholds.

The results for Laminar burning speed of Syngas-Air mixtures compare well with other data available and confirms the method s and analysis used for syngas mixtures are accurate. For Syngas-O_2-He the literature data is very sparse and there is enormous variation in the gas compositions used by others. The compositions of Syngas used in this study (α=5,10,25%) are relevant to practical engineering applications for Hydrogen enrichment in IC engine and therefore we, accept the data to be of good value. The ratio of He to O_2 is the same as typical air, therefore only the specific heat capacity was effected and needs to be adjusted in engineering applications of this data.

The Heptane auto-ignition study was performed to serve as confirmation of the methods of this study. The results agree well with the literature as indicated in section 5.5. Furthermore, the technique used here seems to be able to detect both the on-set of auto-ignition and the conditions for ignition delays < 1ms. For GTL (S8) comparative data is scarce, however the existing data

seems to indicate that the results of this study follow the correct trends for both the onset of auto-ignition and 1ms ignition delay.

6.2 Recommendations for future work

The laboratory facility, the modelling and data analysis all function reasonably well, but there is a lot of room for improvements in streamlining and making the processes more seamless. An area that would benefit from immediate improvements is the data handling. The current procedures require a tedious handling of the data that is heavily operator dependent and therefore prone to errors. The following are suggested improvements to the data handling and processing:

- The LabVIEW DAQ system can be made to automatically label the file name with pertinent information about the data run, as to not burden the operator to rename and store the file in an appropriate folder.

- By using a consistent file naming scheme, a Matlab program can be written to automatically extract the raw data created by LabVIEW and present the data to the user for cropping and visual evaluation.

- The data analysis is currently executed in two major steps. One step involves a Fortran subroutine to interact with STANJAN (chemical equilibrium code) in order to solve the two conservation equations. The second step involves analyzing the output of the first step which is essentially the mass fraction burned into LBS, or MBR, this is typically done in Matlab or Excel. A better approach would be using Matlab to invoke STANJAN directly, therefore, eliminating the first step and achieving the final result in a very convenient format (Matlab file).

- The data fitting portion of the analysis has been improved by the author by modifying a Matlab program first developed by Omid Oskar. This new program concatenates the

results from individual data files selected by the user, into a single lot ready for fitting to a desired correlation. However, a user friendly graphical interface would be a great next step to improving this program.

The mechanical parts of the laboratory require constant maintenance and upkeep, but these tasks are not typically scheduled, but rather repaired as needed. In high temperature experiments and when handling liquid fuel, a schedule maintenance plan would alleviate interruptions in the testing. Extended spark plug electrodes, ionization probes and valves are usually the sources of leaks and issues with the vessel and manifold. Having replacement items and/or repair kits for the valves is the best corrective action for this issue. In high temperature and liquid fuel testing the valves should be repacked (rebuilt) every ~16 hours of operation. The extended spark plug electrodes should be replaced and/or inspected every 20 runs and the vessel cleaned every ~15 runs.

Other areas of improvements that can improve or extend the operational range of the facility are:

- A higher temperature pressure transducer will enable higher initial temperature up to 325C (~ 600K) using a Kalrez O-ring to seal the vessel, however the current ionization probes may not be used. The wires to the vessel would need to be routed in a Teflon or metal jacket and actively cooled with air, similar to is done currently for the pressure transducer.

- Improve sealing for spherical chamber oven, would improve the heat up time of the spherical vessel, and make the environment in the test facility more comfortable. In addition, strap on band heaters could be used to further improve the heat up time of the vessel.

- A more extreme improvement to the facility would be a computer controlled filling system using microprocessor controlled solenoid valves in the filling manifold.

- The ionization probe design can be improved by replacing the sensing rod with a headed rod therefore avoiding the potential for the rod to be pushed outward by the high internal pressure in the vessel. This will also increase the sensing surface area and will likely create a better seal.

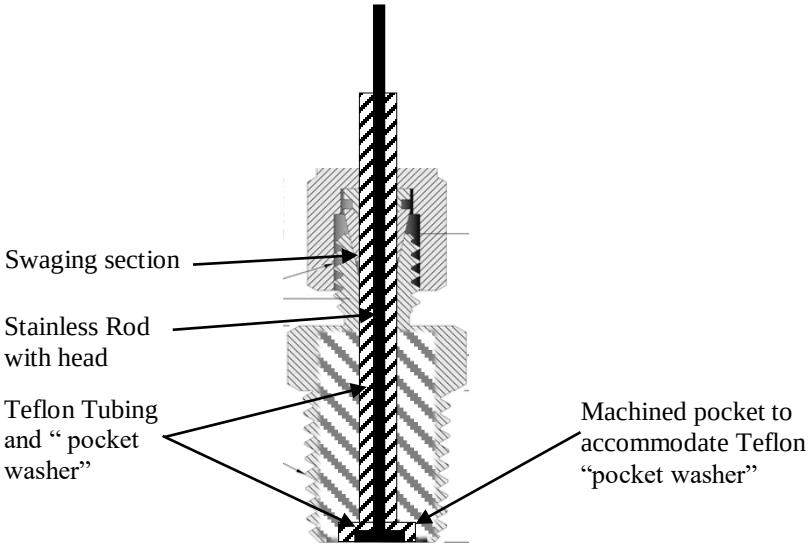

- During auto-ignition and all combustion testing the pressure in the vessel is monotonically increasing thus producing transient test conditions. This is great for laminar burning speed, mass burning rate determination since each experiment provides many data point at varying conditions. For auto-ignition studies, since the conditions in the constant volume vessel are transient, the only measurable parameter is the onset of auto-ignition, which is the instant where the pressure data becomes oscillatory. However, it is also desirable to measure the ignition delay of a combustible mixture especially since this a parameter typically reported by other studies and used in the engineering community. The measurement of the ignition delay requires that the pressure be increased to a desired value then leveled off until auto-ignition occurs, this is typically accomplished with very sophisticated rapid compression machines. It may be possible to modify the existing facility, to achieve the required test conditions from the constant volume experiments and therefore extract the ignition delay data. To accomplish a levelling pressure condition thus maintaining steady condition for a

certain duration of the test, the ignition point in the vessels can be tuned. By raising the ignition point closer to the top surface of the vessel and/or by adding multiple ignition points, one can tune the arrival time of the flame front to the top surfaces of the vessel. Once part of the flame front reaches a vessel's surface, that portion of the flame is quenched and the flame front gases are cooled due to the heat transfer to the vessel's wall. This "controlled flame quenching" can be used to reduce and control the pressure rise in the vessel. The amount of area of flame front that contacts the vessel surface can be easily tuned by the location of the ignition point and therefore the amount of impact on the pressure rise can be controlled. This technique should provide the opportunity to control the shape of the pressure rise in a constant volume vessel thus producing the required conditions for measuring the ignition delay.

7.0 REFERENCES

[1] M. Metghalchi and J. C. Keck, "Burning Velocities of Mixtures of Air with Methanol, Isooctane, and Indolene at High Pressure and Temperature," *Combustion and Flame,* vol. 48, pp. 191-210, 1982.

[2] M. M. a. J. C. Keck, "M. Metghalchi and J. C. Keck, "Burning Velocities of Mixtures of Air with Methanol, Isooctane, and Indolene at High Pressure and Temperature," *Combustion and Flame,* vol. 48, pp. 191-210, 1982.

[3] T. Scholte and P. Vaags, "Burning velocities of mixtures of hydrogen, carbon monoxide and methane with air," *Combustion and Flame,* vol. 3, pp. 511-524, 1959.

[4] G. Mittal, C.-J. Sung and R. A. Yetter, "Autoignition of H2/CO at elevated pressures in a rapid compression machine," *International Journal of Chemical Kinetics,* vol. 38, no. 8, pp. 516-529, 2006.

[5] H. Sun, S. I. Yang, G. Jomaas and C. K. Law, "High-pressure laminar flame speeds and kinetic modeling of carbon monoxide/hydrogen combustion," *arbon monoxide/hydrogen combustion,* vol. 31, no. 1, pp. 439-446, 2007.

[6] J. J. Marano, "Refinery Technology Profiles: Gasification and Supporting Technologies," *U.S. Department of Energy National Energy Technology Laboratory Energy Information Administration,* 2003.

[7] N. O. Elbashir and F. T. Eljack, "A Method to Design an Advanced Gas-to-Liquid Technology Reactor for Fischer-Tropsch Synthesis," *Advances in Gas Processing,* pp. 369-377, 2010.

[8] H. Sajjad, "Comparative Study of Biodiesel, GTL Fuel and Their Blends in Context of Engine Performance and Exhaust Emission," *Procedia Engineering,* vol. 90, pp. 466-471, 2014.

[9] T. G. S. a. P. B. Vaags, "The influence of small quantities of hydrogen and hydrogen compounds on the burning velocity of carbon monoxide-air flames," *Combustion and Flame,* vol. 3, pp. 503-510, 1959.

[10] M. P. Burke, M. Chaos, F. L. Dryer and Y. Ju, "Negative pressure dependence of mass burning rates of H2/CO/O2/diluent flames at low flame temperatures," *Combustion and Flame,* vol. 157, no. 4, pp. 618-631, 2010.

[11] C. Vagelopoulos and F. Egolfopoulos, "Laminar flame speeds and extinction strain rates of mixtures of carbon monoxide with hydrogen, methane, and air," *Symposium (International) on Combustion,* vol. 25, no. 1, pp. 1317-1323, 1994.

[12] J. Natarajan, Y. Kochar, T. Lieuwen and J. Seitzman, "Pressure and preheat dependence of laminar flame speeds of H2/CO/CO2/O2/He mixtures," *Proceedings of the Combustion Institute,* vol. 32, no. 1, pp. 1261-1268, 2009.

[13] Y. Zhang, W. Shen, M. Fan and H. Zhang, "Laminar flame speed studies of lean premixed H2/CO/air flames," *Combustion and Flame,* vol. 161, no. 10, pp. 2492-2495, 2014.

[14] H. C. Lee, L. Y. Jiang and A. A. Mohamad, "A review on the laminar flame speed and ignition delay time of Syngas mixtures," *International Journal of Hydrogen Energy,* vol. 39, no. 2, pp. 1105-1121, 2014.

[15] P. Pal, A. B. Mansfield, M. S. Wooldridge and H. G. Im, "Characteristics of Syngas Auto-ignition at High Pressure and Low Temperature Conditions with Thermal Inhomogeneities," *Energy Procedia,* vol. 66, pp. 1-4, 2015.

[16] S. Gersen, H. Darmeveil and H. Levinsky, "The effects of CO addition on the autoignition of H2, CH4 and CH4/H2 fuels at high pressure in an RCM," *Combustion and Flame,* vol. 159, no. 12, pp. 3472-3475, 2012.

[17] C. Dong and Q. Zhou, "Experimental study on the laminar flame speed of hydrogen/carbon monoxide/air mixtures," *Fuel,* vol. 88, no. 10, pp. 1858-1863, 2009.

[18] A. Kéromnès, "An experimental and detailed chemical kinetic modeling study of hydrogen and syngas mixture oxidation at elevated pressures," *Combustion and Flame,* vol. 160, no. 6, pp. 995-1011, 2013.

[19] G. E. Andrews and D. Bradley, "The Burning Velocity of Methane Air Mixtures," *Combustion and Flame,* vol. 19, no. 2, pp. 275-288, 1972.

[20] C. J. Rallis and A. M. Garforth, "The determination of laminar burning velocity," *Progress in Energy and Combustion,* vol. 6, no. 4, pp. 303-329, 1980.

[21] A. Moghaddas, K. E. Far and H. Metghalchi, "Laminar burning speed measurement of premixed n-decane/air mixtures using spherically expanding flames at high temperatures and pressures," *Combustion and Flame,* vol. 159, no. 4, pp. 1437-1443, 2012.

[22] D. Lee and S. Hochgreb, "Hydrogen autoignition at pressures above the second explosion limit (0.6–4.0 MPa)," *International Journal of Chemical Kinetics,* vol. 30, no. 6, pp. 385-406, 1998.

[23] C. Prathap and A. Ray, "Investigation of nitrogen dilution effects on the laminar burning velocity and flame stability of syngas fuel at atmospheric condition," *Combustion and Flame,* vol. 155, no. 1-2, pp. 145-160, 2008.

[24] L. D. Thi, Y. Zhang and Z. Huang, "Shock tube study on ignition delay of multi-component syngas mixtures – Effect of equivalence ratio," *International Journal of Hydrogen Energy,* vol. 39, no. 11, pp. 6034-6043, 2014.

[25] K. E. Far, F. Parsinejad and H. Metghalchi, "Flame structure and laminar burning speeds of JP-8/air premixed mixtures at high temperatures and pressures," *Fuel,* vol. 89, no. 5, pp. 1041-1049, 2010.

[26] T. M. Vu, J. Park, J. S. Kim and O. B. Kwon, "Effects of hydrocarbon addition on cellular instabilities in expanding syngas–air spherical premixed flames," *International Journal of Hydrogen Energy,* vol. 34, no. 16, pp. 6961-6969, 2009.

[27] A. K. d. a. C.-J. Sung, "Ignition Delay Study of Moist Syngas/Oxidizer and Hydrogen/Oxidizer Mixtures using a Rapid Compression Machine," in *49th AIAA Aerospace*

Sciences Meeting including the New Horizons Forum and Aerospace Exposition, Orlando, 2011.

[28] M. I. Hassan, K. T. Aung and G. M. Faeth, "Markstein numbers and unstretched laminar burning velocities of wet carbon monoxide flames," *American Institute of Aeronautics and Astronautics*, 1996.

[29] O. Askari and A. A. K. V. B. A. Ali Moghaddas, "Laminar burning speed measurement and flame instability study of H2/CO/air mixtures at high temperatures and pressures using a novel multi-shell model," *Combustion and Flame (2016)*, p. http://dx.doi.org/10.1016/j.combustflame.2016.03.018, 2016.

[30] S. N. a. Y. Z. J. Zhang, "Experimental and modeling study of the auto-ignition of n-heptane/n-butanol mixtures," *Combustion and Flame*, vol. 160, no. 1, pp. 31-39, 2013.

[31] R. D. Sante, "Measurements of the auto-ignition of n-heptane/toluene mixtures using a rapid compression machine," *Combustion adn Flame*, vol. 159, no. 1, pp. 55-63, 2012.

[32] J. C. S. L. a. S. S. H. An, "The effects of hydrogen addition on the auto-ignition delay of homogeneous primary reference fuel/air mixtures in a rapid compression machine," *International Journal of Hydrogen Energy*, vol. 40, no. 40, pp. 13994-14005, 2015.

[33] S. Jerzembeck, N. Peters, P. Pepiot-Desjardins and H. Pitsch, "Laminar burning velocities at high pressure for primary reference fuels and gasoline: Experimental and numerical investigation," *Combustion and Flame*, vol. 156, pp. 292-301, 2009.

[34] P. Dagaut, "Experimental and detailed kinetic model for the oxidation of a Gas to Liquid (GtL) jet fuel," *Combustion and Flame*, vol. 161, no. 3, pp. 835-847, 2014.

[35] S. Dooley, S. H. Won, M. Chaos, J. Heyne, Y. Ju, F. L. Dryer, K. Kumar, C.-J. Sung, H. Wang, M. A. Oehlschlaeger and R. J. Santoro, "A jet fuel surrogate formulated by real fuel properties," *combustion and flame*, vol. 157, pp. 2333-2339, 2010.

[36] K. K. a. C.-J. sung, "Autoignition of Jet Fuels under High Pressure and Low-to-intermidiate Temperatures," in *47th AIAA Aerospace Sciences Meeting Including The New Horizons Forum and Aerospace Exposition*, Orlando, 2009.

[37] A. Moghaddas, *Laminar Burning Speed Measurement, Autoignition and Flame Structure Study of Spherically Expanding Flames*, Boston: PhD Thesis, 2015.

8.0 APPENDIX 1

Newton-Raphson Method

The following equations are to be solved at time step n:

$$\frac{V}{m}+\frac{A\delta}{m}=\sum_{i=0}^{n-1}v_{bi}x_i+v_{bn}x_n+(1-\sum_{i=0}^{n-1}x_i-x_n)v_u \tag{17}$$

$$\frac{E}{m}-\frac{Q}{m}=\sum_{i=0}^{n-1}e_{bi}x_i+e_{bn}x_n+(1-\sum_{i=0}^{n-1}x_i-x_n)e_u \tag{18}$$

x_n, e_{bn} and v_{bn} are unknowns, and e_{bn} and v_{bn} are functions of temperature T_{bn}.

Defining F_1 and F_2:

$$F_1=\frac{V}{m}+\frac{A\delta}{m}-\sum_{i=0}^{n-1}v_{bi}x_i-v_{bn}x_n-(1-\sum_{i=0}^{n-1}x_i-x_n)v_u \tag{1a}$$

$$F_2=\frac{E}{m}-\frac{Q}{m}-\sum_{i=0}^{n-1}e_{bi}x_i-e_{bn}x_n-(1-\sum_{i=0}^{n-1}x_i-x_n)e_u \tag{2a}$$

Differentiate F_1 and F_2 with respect to x_n and T_{bn}

$$A_{11}=\frac{\partial F_1}{\partial x}=-v_{bn}+v_u$$

$$A_{12}=\frac{\partial F_1}{\partial T_{bn}}=-\frac{R_{bn}}{p} \tag{3a,4a,5a,6a}$$

$$A_{21}=\frac{\partial F_2}{\partial x}=-e_{bn}+e_u$$

$$A_{22}=\frac{\partial F_2}{\partial T_{bn}}=-C_{v_{bn}}$$

Rb_n = gas constant of burned gas in the nth shell

$C_{v_{bn}}$= constant volume specific heat of the burned gas in the nth shell

"A" forms the Jacobian matrix.

The following system of linear equations is solved for dx_n and dT_{bn}:

$$\begin{bmatrix} A_{11} & A_{12} \\ A_{21} & A_{22} \end{bmatrix} \begin{bmatrix} dx_n \\ dT_{bn} \end{bmatrix} = \begin{bmatrix} -F_1 \\ -F_2 \end{bmatrix} \tag{7a}$$

Increment x_n and T_{bn} by dx_n and dT_{bn} respectively and use new values to check convergence of equations 17 and 18 iteratevely solve and increment x_n and T_{bn} until convergence is achived. Convergence of equations 17 and 18 was carefully analyzed and was found that equation 18 has a lower tollerance to small changes of x_n and T_{bn} therefore it was used to check for convergence of both equations. The convergence was determined based on how close F_2 was to value zero it was found that 0.01gave excellent results with a relatively small number of iterations. Values of 0.0000001 produced insignificantly small variations in x_n with a very large number of iterations.

9.0 APPENDIX 2

Flame stretch rate effects on LBV are analyzed in this appendix. Flame stretch rate is defined as: $\alpha = \frac{1}{A}\frac{dA}{dt} = 2\frac{\dot{r}}{r}$ For spherical flames.

Where: A is the flame area, r is the flame radius and t = time.

Results of calculations of the flame stretch rate of a typical experimental run are shown below.

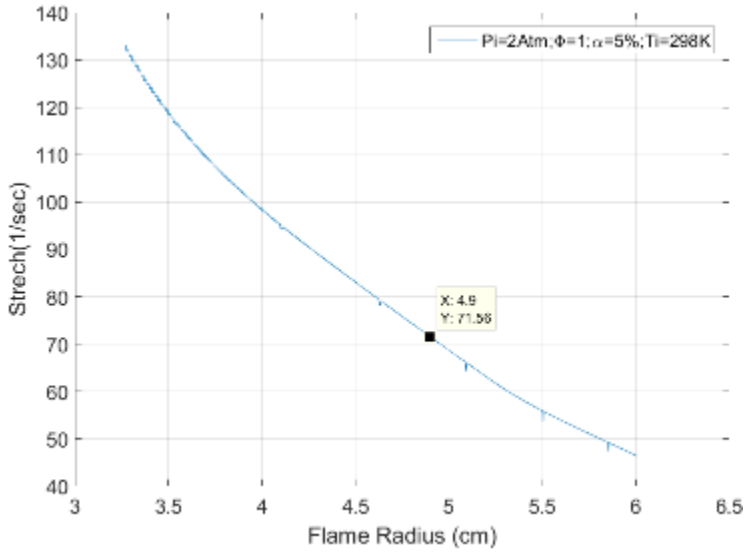

From the graph above it can be seen that flame stretch rate drastically decreases with increasing flame radius. "*For stretch rates lower than 70 1/s, the burning speed is not affected by stretch. Numerous studies have shown that stretch rates higher than 100 1/s can affect the laminar burning speeds (Egolfopoulos, Du et al. 1992, Hara and Tanoue 2006, Liao, Jiang et al. 2007, Bradley, Lawes et al. 2009).* " (Ali Moghaddas Phd thesis) [37]

10.0 APPENDIX 3

JANAF table coefficients for specific heat and specific energy calculations of the unburned gas used in equations 11 and 12.

$$C_p = R\left(c_0 + c_1 T + c_2 T^2 + c_3 T^3 + c_4 T^4\right) \tag{11}$$

$$e_u = \left(c_0 + c_1 \frac{T}{2} + c_2 \frac{T^2}{3} + c_3 \frac{T^3}{4} + c_4 \frac{T^4}{5} + \frac{c_5}{T}\right) RT - RT \tag{12}$$

Table of JANAF coefficient examples used in evaluation of unburned gas properties.

	c_0	c_1	c_2	c_3	c_4	c_5	c_6
O2	3.212936	0.001127	-5.8E-07	1.31E-09	-8.8E-13	-1005.25	6.034737
N2	3.298677	0.001408	-4E-06	5.64E-09	-2.4E-12	-1020.9	3.950372
AR	2.5	0	0	0	0	-745.375	4.366
CO2	2.275724	0.009922	-1E-05	6.87E-09	-2.1E-12	-48373.1	10.18849

Molar Averaging:

$$C_{p(mixture)} = \sum_{i=1}^{\cdots} C_{pi} n_i \tag{6a}$$

Where:

C_{pi} = specific heat of the ith species in the mixture

n_i = mole fraction of the ith species in the mixture

and C_{pi} is computed using equation 11.

$$e_{u(mixture)} = \sum_{i=1}^{\cdots} e_{ui} n_i \tag{6b}$$

Where:

e_{ui} = specific internal energy of the ith species in the mixture

n_i = mole fraction of the ith species in the mixture

and e_{ui} is computed using equation 12.

11.0 APPENDIX 4

List of publications resulting from the laboratory facility described in this study:

Journal Publications:

1. Elia, M., Ulinski, M. and Metghalchi, M., "Laminar Burning Velocity of Methane-Air-Diluent Mixtures". ASME Journal of Engineering for Gas Turbines and Power, January 2001, Vol.123, 190-196.

2. Rahim, F., Elia, M., Ulinski, M., and Metghalchi, M., "Burning Velocity Measurements of Methane-Oxygen-Argon Mixtures and an Application to Extend Methane-Air Burning Velocity Measurements". International Journal of Engine Research 2002, Vol. 3, No. 2, 81-92

3. Farsinejad, F., Matlo, M. and Metghalchi, M., "A Mathematical Model for Schlieren and Shadowgraph Images of Transient Expanding Spherical Thin Flames". ASME Journal of Engineering for Gas Turbines and Power, April 2004, Vol. 126, 241-247.
4. Numerical Results of a Single Submerged Attached Growth Bioreactor (SAGB) for Simultaneous Oxidation of Organics and Nitrogen Removal", Water Science and Technology **52**(7), 97-105, 2005.

5. Parsinejad, F, Arcari, C. and Metghalchi, H., "Flame Structure and Burning Speed of JP-10 Air Mixtures" Combustion Science and Technology, 178: 975-1000, 2006.

6. Pedros, P. B., Wang, J. Y. and Metghalchi, H. "A single Submerged Attached Growth Bioreactor for Simultaneous Removal of Organics and Nitrogen", Journal of Environmental Engineering, pp191-197, February 2007.

7. Parsinejad, F., Keck, J.C. and Metghalchi, H., "On the Location of Flame Edge in Shadowgraph Pictures of Spherical Flames; Experimental and Theoretical Study", Experiments in Fluids, Volume 43, Number 6: 887-894, December 2007.

8. Rahim, F., Eisazadeh Far, K., Parsinejad, F., Adrews, R. J. and Metghalchi, H., "A Thermodynamic Model to Calculate Burning Speed of Methane-Air- Diluent Mixtures", Int. J. of Thermodynamics, Vol. 11 (No. 4), pp. 151-160, December 2008.

9. Eisazadeh-Far, K., Parsinejad, F., and Metghalchi, H., "Flame Structure and Laminar Burning Speeds of JP-8/Air Premixed Mixtures at High Temperatures and Pressures" Fuel 89 (2010) 1041-1049.

10. Eisazadeh-Far, K., Parsinejad, F., Metghalchi, H., and Keck, J. C., "A Thermodynamic Model for Argon Plasma Kernel Formation". Int. J. Of Thermodynamics, Volume 13, No. 4 pp119-126, December 2010.

11. Eisazadeh-Far, K., Parsinejad, F., Metghalchi, H., and Keck, J.C., "On Flame Kernel Formation and Propagation in Premixed Gases". Combustion and Flame, 2010, 157: 2211-2221.

12. Eisazadeh-Far, K., Moghaddas, A., Rahim, F., and Metghalchi, H. "Burning Speed and Entropy Production Calculation of a Transient Expanding Spherical Laminar Flame Using a Thermodynamic Model", Entropy 2010, 12, 2485-2496; doi:10.3390/e12122485.

13. Eisazadeh-Far, K., Moghaddas, A., Al-Mulki, J., and Metghalchi, H., "Laminar Burning Speeds of Ethanol/Air/Diluent Mixtures". Proceedings of the Combustion Institute, Volume 33, Issue 1, 2011, Pages 1021 – 1027.

14. Eisazadeh-Far, K., Moghaddas, A., Metghalchi, H., and Keck, J. C., "The Effect of Diluent on Flame Structure and Laminar Burning Speed of JP-8/Oxidizer/Diluent Premixed Flames'. Fuel 90 (2011) 1476-1486.

15. Eisazadeh-Far, K., Metghalchi, H., and Keck, J.C., "Thermodynamic properties of Ionized Gases at High Temperatures". ASME Journal of Energy Resources and Technology, June 2011, Vol. 133.

16. Moghaddas, A., Eisazadeh-Far, K., and Metghalchi, M., "Laminar Burning Speed Measurement of Premixed n-decane/air Mixtures Using Spherically Expanding Flames at High Temperatures and Pressures". Combustion and Flame 159 (2012) 1437-1443.

17. Moghaddas, A., Bennett, C., Eisazadeh-far, K. and Metghalchi, H, "Measurement of Laminar Burning Speed and Determination of Onset of Autoignition of Jet-A/Air and JP-8/Air Mixtures in a Constant Volume Spherical Chamber". ASME Journal of Energy Resources Technology, June 2012, Vol. 134.

18. Askari, O., Metghalchi, M., Moghaddas, A., Hannani, S. K., and Ebrahimi, R., "Fundamental Study Of Spray and Partially Premixed Combustion Characteristics of Methane/Air Mixture". ASME Journal of Energy Resources Technology, June 2013, Vol135 No. 2 021001.

19. Janbozorgi, M., Sheikhi, M. R. H. and Metghalchi, H., "Principle of Detailed Balance and the Second Law of Thermodynamics in Chemical Kinetics". *ASME J. Energy Resour. Technol*. Vol 135, (2013).

20. Moghaddas, A., Bennett, C., Rokni, E. and Metghalchi, H., "Laminar Burning Speeds and Flame Structures of Mixtures of Difluoromethane (HFC-32) and 1,1-Difluoroethane (HCF-152a) with Air at Elevated Temperatures and Pressures", HVAC&R Research 20 (2014) 42-50.

21. Askari, O., Metghalchi, H., Hannani, S.K., Hemmati, H. and Ebrahimi, R., "Lean Partially Premixed Combustion Investigation of Methane Direct-Injection under Different Characteristic Parameters". ASME Journal of Energy Resources Technology, June 2014, Vol. 136/022202-1

22. Rokni, E., Mossadagh, A., Askari, O. and Metghalchi, H., "Measurement of Laminar Burning Speed and Investigation of Flame Stability of Acetylene (C_2H_2)/air Mixtures". ASME Journal of Energy Resources Technology, January 2015, Vol. 137/012204-1

23. Askari, O., Janbozorgi, M., Greig, R., Moghaddas, A., and Metghalchi, H., "Developing Alternative Approaches to Predicting the Laminar Burning Speed of Refrigerants Using the Minimum Ignition Energy". Science and Technology for the Built Environment, 21:2 220-227, 2015

Conference Papers

1. Ulinski, M. Moore, P. Elia, M. and Metghalchi, M. "Laminar Burning Velocity of Methane-Air-Diluent Mixtures" Proceeding of the ASME Internal Combustion Engine Division, Fort Lauderdale, Florida, ICE-Vol. 30-3, 1998.

2. Elia, M., Moore, P., Ulinski, M., and Metghalchi, M., "Laminar Burning Velocity of Methane-Oxygen-Argon (CH_4-O_2-Ar) Mixtures". Proceedings of the ASME Internal

Combustion Engine Division, Columbus Indiana, ICE-Vol. 32-2, 1999.

3. Ulinski, M., Li, Z., Elia, M., Fletcher, C., and Metghalchi, M., "Burning Velocity Measurements in Micro-Gravity Conditions". Proceedings of 1999 Eastern States Section of the Combustion Institute Meeting, North Carolina State University, October 11-13, 1999.

4. Rahim, F and Metghalchi, M., "Burning Velocity Measurements in Micro-Gravity Conditions". Proceedings of 4th International Conference of ISME, May 16-19, 2000.

5. Rahim, F., Ulinski, M., and Metghalchi, M., "Burning Velocity Measurements in Spherical and Cylindrical Vessels". Proceedings of 5th International Conference of ISME, May 27-29, 2001.
6. Rahim, F., and Metghalchi, M., "Burning Velocity for Spherical Flames in Cylindrical and Spherical Chambers". Proceedings of 2001 Eastern States Section of the Combustion Institute Meeting, South Carolina, December 3-5, 2001.

7. Rahim, F., Metghalchi, M. and Keck, J.C., "Development of Reaction Mechanism and Measurement of Laminar Burning Speeds of Methane/Oxidizer/Diluent Mixtures at Low Temperature and High Pressures". Western States Section of the Combustion Institute Meeting, California, March 2002

8. Matlo, M., Parsinejad, F., and Metghalchi, M., "Schlieren and Shadowgraph Images of Transient Expanding Spherical Thin Flames". Proceedings of IMECE2002-34318: ASME International Mechanical Engineering Congress & Exposition, November 17-22, New Orleans, Louisiana.

9. Kahraman, S., Parsinejad, F., Metghalchi, M., and Fiveland, S., "Burning Speed Measurements of Mixtures of Methane/Ethane/Propane/Butane with Air". Proceedings of The Third Joint Meeting of the US Sections of The Combustion Institute, University of Illinois at Chicago, March 16-19, 2003

10. Rahim, F., Metghalchi, M. and Keck, J.C., "Regions of Instabilities in Outwardly Propagating Methane-Oxidizer-Diluent Mixtures". Proceedings of Western States Section of the Combustion Institute 2003 Fall Meetings, UCLA, October 2003.

11. Parsinejad, F., and Metghalchi, M., "An Investigation on Burning Speed of JP-10 Air Mixtures at High Temperature and Pressure". Proceedings of 2003 Technical Meeting of Eastern States Section of The Combustion Institute, Pennsylvania State University, October 2003

12. Parsinejad, F., Arcari, C., Shirk, E., and Metghalchi, H., "Burning Speed Measurement of JP-8 Air Flames", IMECE2004-61573, Proceedings of IMECE'04, 2004 ASME International Mechanical Engineering Congress & Exposition, November 2004, Anaheim, California.

13. Parsinejad, F., Arcari, C., Shirk, E., and Metghalchi, H., "Optical Investigation of Outwardly Expanding Spherical Flames" Proceedings of The Fourth Joint Meeting of the US Sections of The Combustion Institute, Drexel University, March 20-23, 2005.

14. Goldthwaite, D., Metghalchi, H., and Keck, J.C., "Refinement of Reduced Chemical Mechanisms for the Modeling of the Rapid Compression Combustion of Heptane and Octane". IMECE2005-81368, Proceedings of IMECE 2005 ASME International Mechanical Engineering Congress & Exposition, November 2005, Orlando, FL.

15. Parsinejad, F., Shirk, E., and Metghalchi, H., "Reformed Fuel and Its properties, Burning Speeds and Flame Characteristics". IMECE2005-80047, Proceedings of IMECE, 2005 ASME International Mechanical Engineering Congress & Exposition, November 2005, Orlando, FL.

16. Parsinejad, F., Shirk, E., Eisazadeh Far, K., and Metghalchi, H., "Laminar Burning Speed Measurements of Premixed JP-8, Oxygen and Helium Flames", Proceedings of 2006 IMECE ASME International Mechanical Engineering Congress & Exposition, November 2006, Chicago, IL.

17. Eisazadeh Far, K., Andrews, R., Parsinejad, F., and Metghalchi, H., "Structure of Fuel/Oxygen/Diluent (Argon, Helium, Nitrogen) Premixed Flames at High Pressures and Temperatures" Proceedings of Eastern States Section of the Combustion Institute, October 2007, University of Virginia.

18. Eisazadeh-Far, K., Parsinejad, F., Gautrea, M., and Metghalchi, H., "Effect of Spark Electrode Geometry on Flame Kernel of Premixed methane-Air Mixtures". IMECE2008-66708, Proceedings of the International Mechanical Engineering Congress and Exposition, Boston, Massachusetts, USA, November 2008.

19. Eisazadeh-Far, K., Parsinejad, F., Gautrea, M., and Metghalchi, H., "Autoignition Study of JP-8/Air Premixed Mixtures" IMECE2008-66711, Proceedings of the International Mechanical Engineering Congress and Exposition, Boston, Massachusetts, USA, November 2008.

20. Eisazadeh-Far, K., Moghaddas, A., Mulki, M., and Metghalchi, H., "Laminar Burning Speeds of Ethanol-Diluent-Air Mixtures" Proceedings of Eastern States Section of the Combustion Institute, October 2009, University of Maryland.

21. Eisazadeh-Far, K., Parsinejad, F. and Metghalchi, H., "A New Model for Flame Kernel Formation and Propagation of Methane-Air Premixed Mixtures" Proceedings of Eastern States Section of the Combustion Institute, October 2009, University of Maryland.

22. Moghaddas, A., Eisazadeh-Far, K. and Metghalchi, H., "Laminar Burning Speeds of Lean n-Decane/Air Premixed Mixtures at High Pressures and Temperatures". Proceedings of the 7th National Technical Meeting of the Combustion Institute, Atlanta, GA March 20-23, 2011

23. Nicolas, G., Janbozorgi, M. and Metghalchi, H., "Combustion Modeling of Methane/Air Mixtures Using the Rate-Controlled Constrained Equilibrium Method". Proceedings of the 7th National Technical Meeting of the Combustion Institute, Atlanta, GA March 20-23, 2011

24. Janbozorgi, M. and Metghalchi, H,. "Rate-Controlled Constrained-Equilibrium (RCCE) Modeling of Expansion of Combustion Products in Supersonic Nozzle". Proceedings of the 7th National Technical Meeting of the Combustion Institute, Atlanta, GA March 20-23, 211.

25. Moghaddas, A., Bennett, C., Eisazadeh-Far, K. and Metghalchi, H., "Burning Speeds and Autoignition of Jet Fuel and JP-8/Air Mixtures". Proceeding of the 2011 ASME International Mechanical Engineering Congress & Exposition, IMECE2011-62292, November 11-17, 2011, Denver Colorado.

26. Moghaddas, A., Askari, O., Rokni, E. and Metghalchi, M, "Measurement of laminar burning speeds and investigation of flame stability of mixtures of H_2/CO with air over a wide range of mixing ratios at high temperatures and pressures" Presented at the 8th US National Combustion Meeting at University of Utah , May 19-22, 2013

27. Rokni, E., Moghaddas, A., Askari, O., and Metghalchi, H. "Measurement of Laminar Burning Speeds and Investigation of Flame Stability of Acytylene (C_2H_2) / air Mixtures" Proceeding of ASME2014 8th International Conference on Energy Sustainability July, Boston, MA- ES-FuelCell 2014-6448